Observational Cosmology

(C. Porciani / K. Basu)

Lecture 8

Cosmology with galaxy clusters

Course website:

http://www.astro.uni-bonn.de/~kbasu/ObsCosmo

Questions?

Mass probes

X-ray
strong lensing

X-ray
SZE
weak lensing

SZE
weak lensing

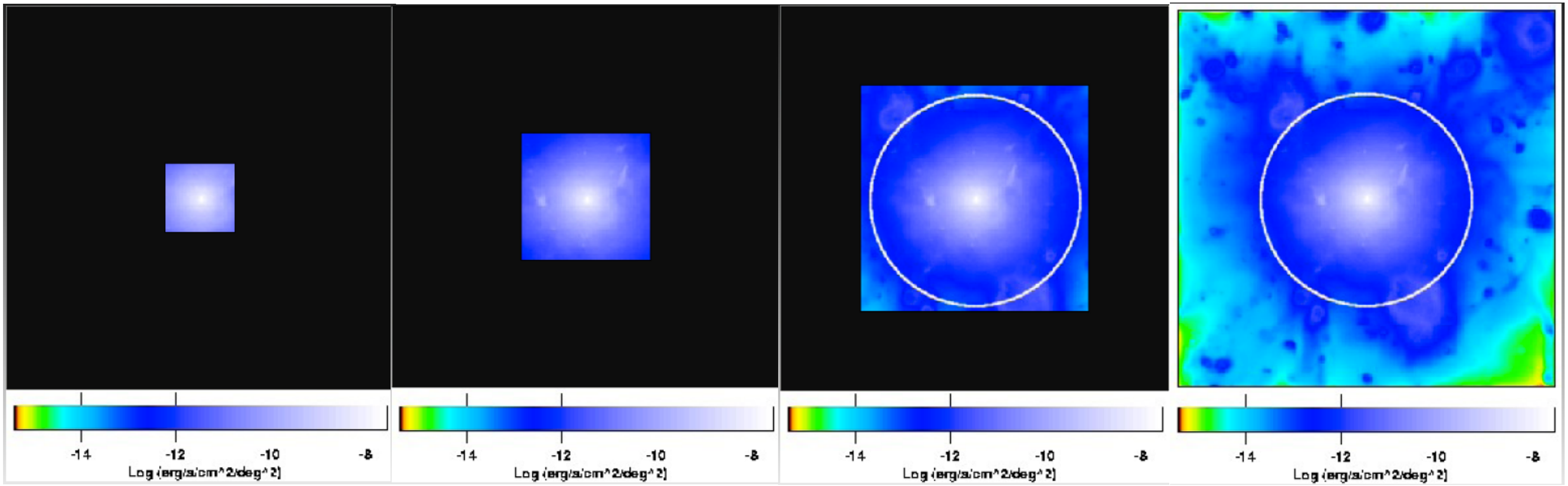

Roncarelli, Ettori et al. 2006

R_{2500}
~ 0.3 R_{200}
~ 0.5 Mpc

R_{500}
~ 0.7 R_{200}
~ 1 Mpc

R_{200}
~ 1.5 Mpc

X-ray view of galaxy clusters

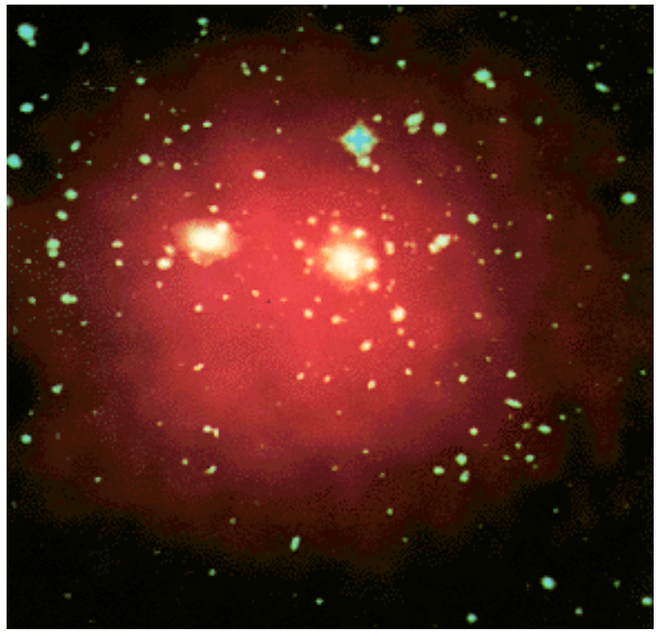

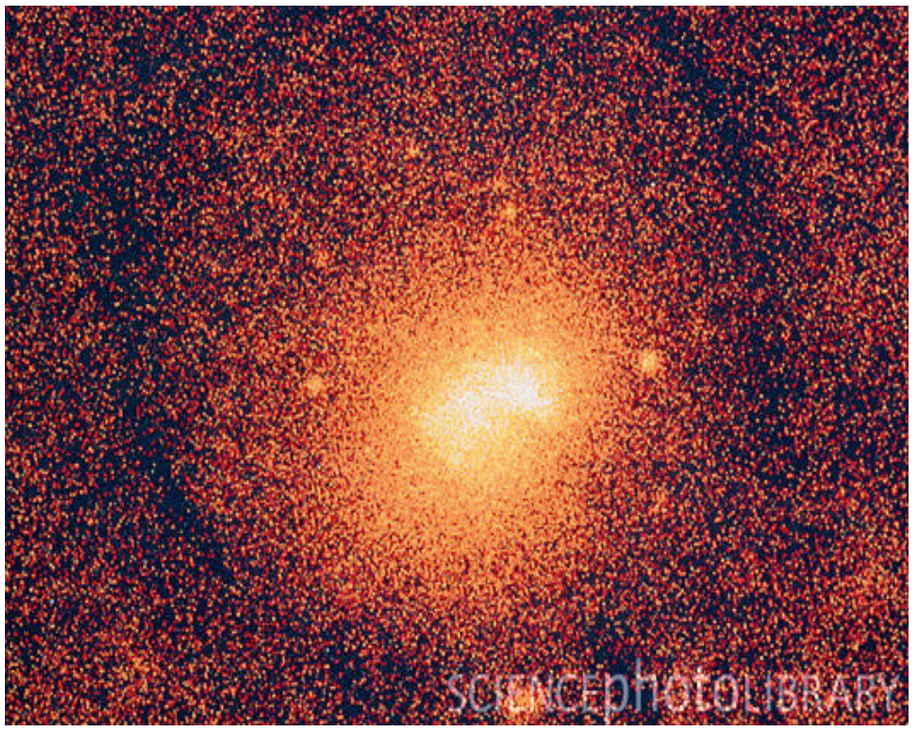

- Most extended X-ray sources in extragalactic fields are galaxy clusters

- Clusters can be identified based on an extent criterion that distinguishes them from AGN, which are 10 times more abundant. This allows a very efficient and clean selection in extragalactic fields (|b|>20deg)

- In deep XMM exposures (>3h) clusters are visible out to z>1

- X-ray selection has a high contrast (n_e^2), allows accurate mass measurements, and search volumes can be quantified

- Additional optical cluster confirmation of a galaxy overdensity is needed

- distance measurements mostly with optical spectroscopy of cluster galaxies

X-ray cluster samples

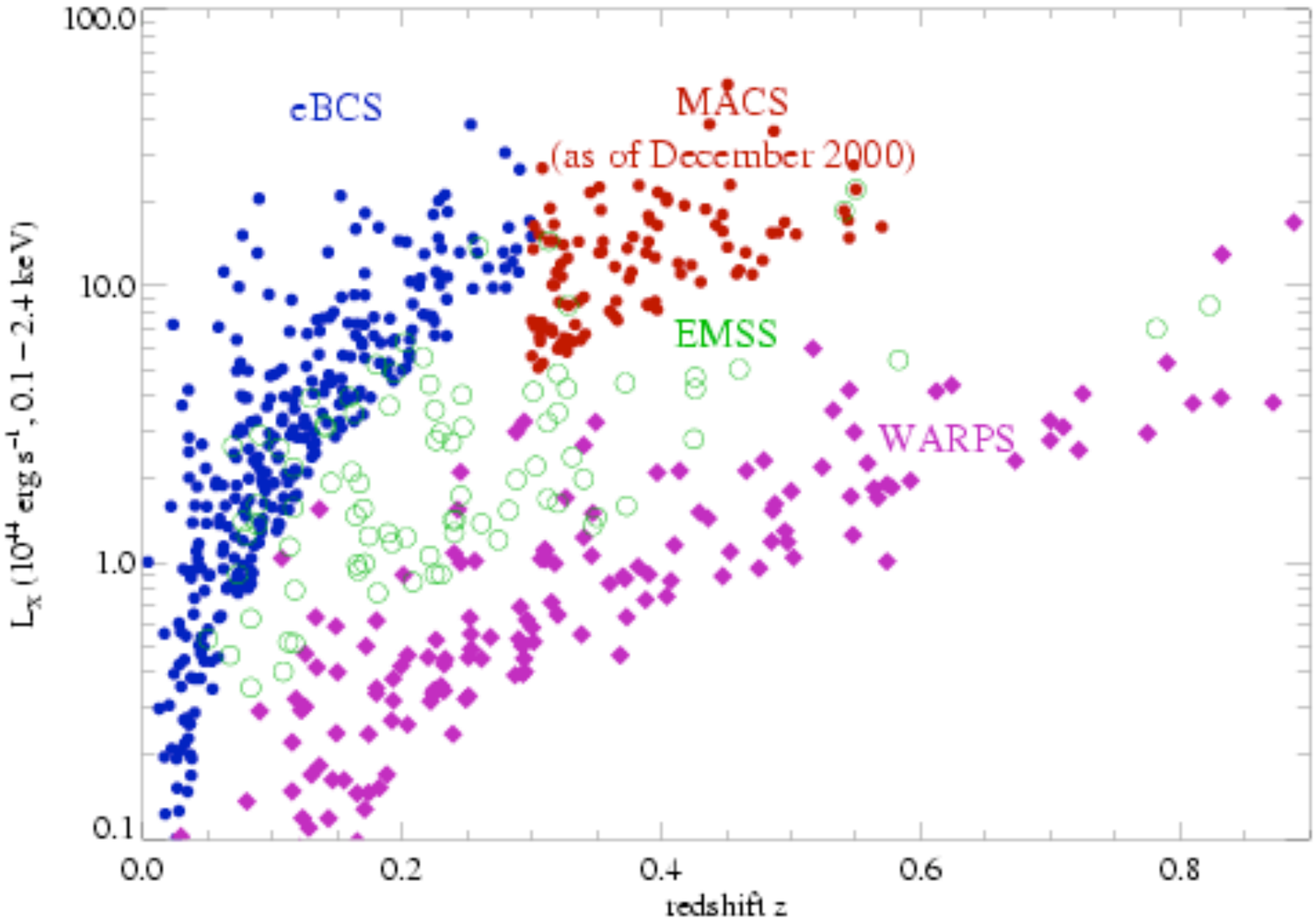

The X-ray flux limit establishes a simple criterion for sample completeness and searching volume, thereby giving a reasonably accurate idea for the number of objects per unit volume.

M–T scaling relation

$$T \propto= \frac{M_{200}}{r_{200}} \propto r_{200}^2 \propto M^{2/3}$$

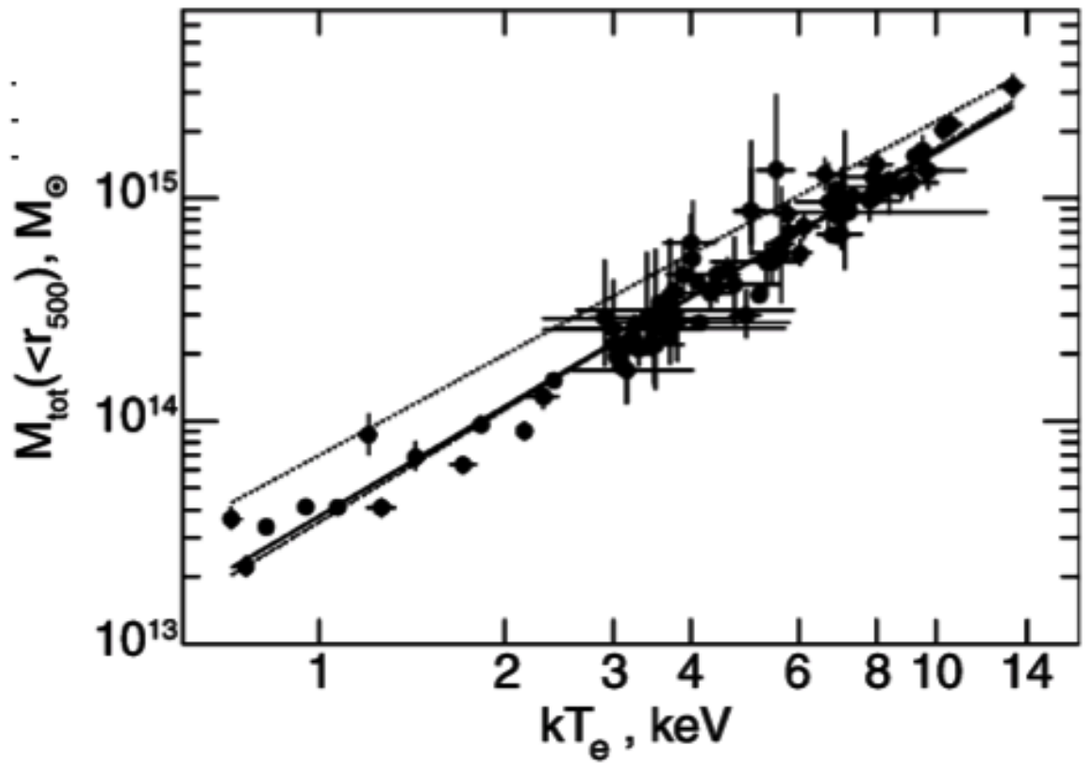

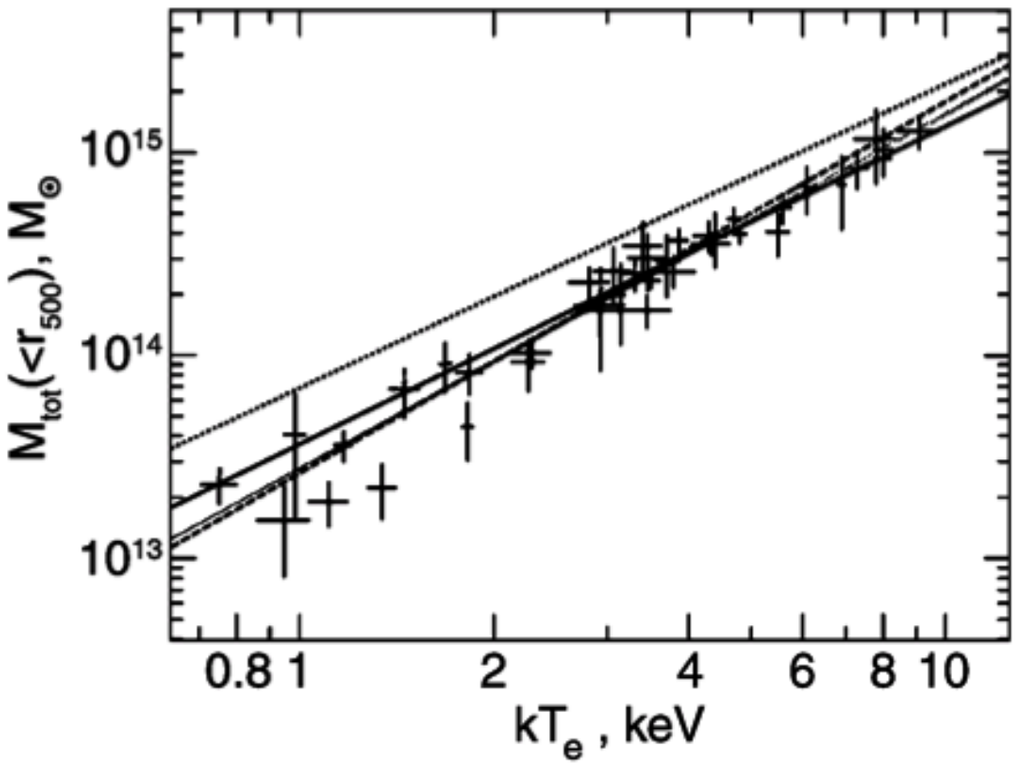

$$M_{500} = 3.57 \times 10^{13}\, M_\odot \left(\frac{kT}{1\,keV}\right)^{1.58}$$

X-ray temperature is good measure of virial mass (better than velocity dispersion).

M–L and L–T relations

$$T \propto= \frac{M_{200}}{r_{200}} \propto r_{200}^2 \propto M^{2/3}$$

From Bremmstrahlung radiation, we have:

$$L_X \propto \rho_g^2 T^{1/2} r_{\rm vir}^3 \propto \rho_g^2 T^{1/2} M_{\rm vir}$$

$$\rho_g \sim M_g r_{\rm vir}^{-3} = f_g M_{\rm vir} r_{\rm vir}^{-3}$$

where $f_g = M_g/M_{vir}$ is the gas fraction.

$$L_X \propto f_g^2 M_{\rm vir}^{4/3} \propto f_g^2 T^2$$

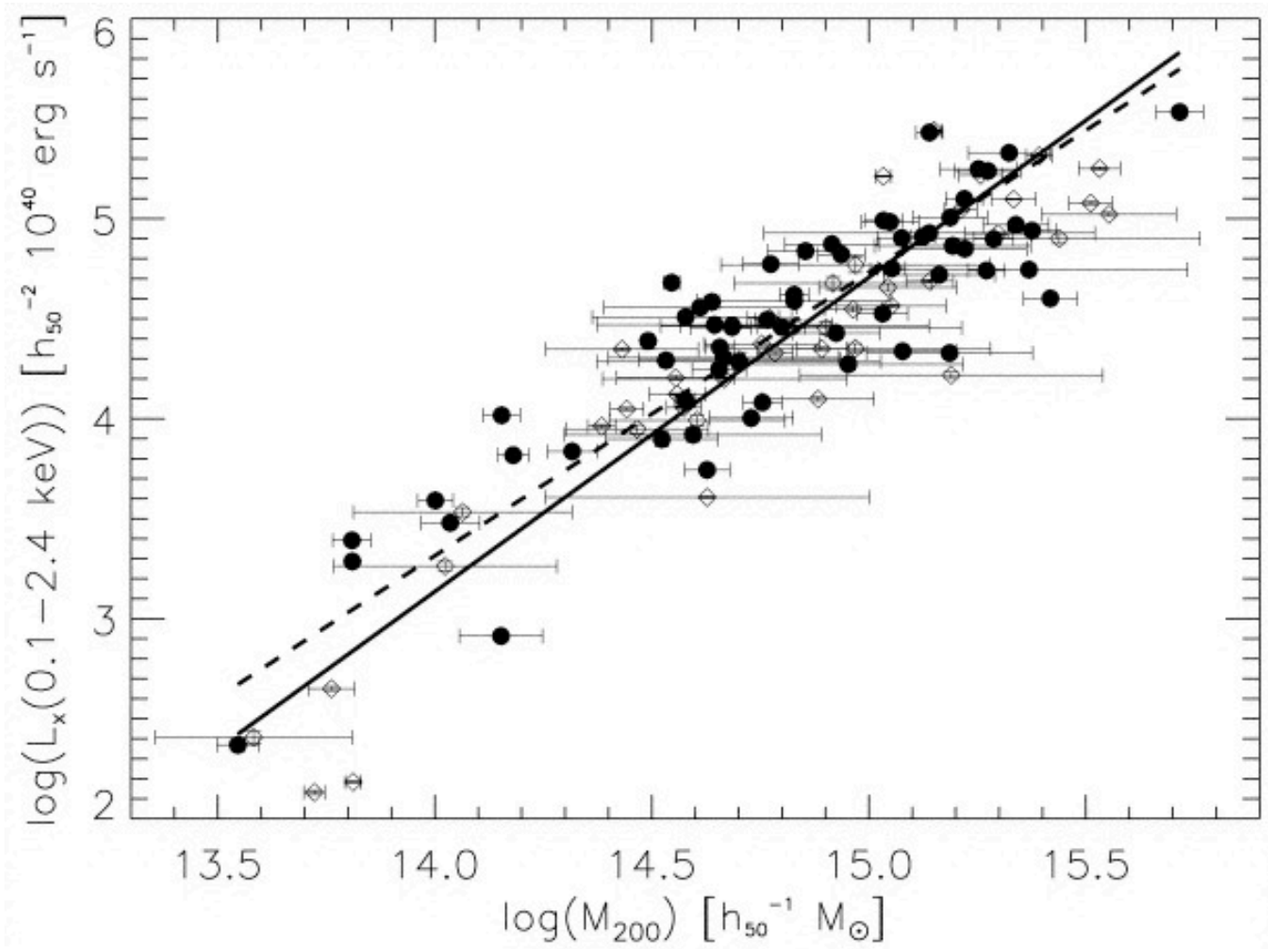

Scaling relation pitfalls

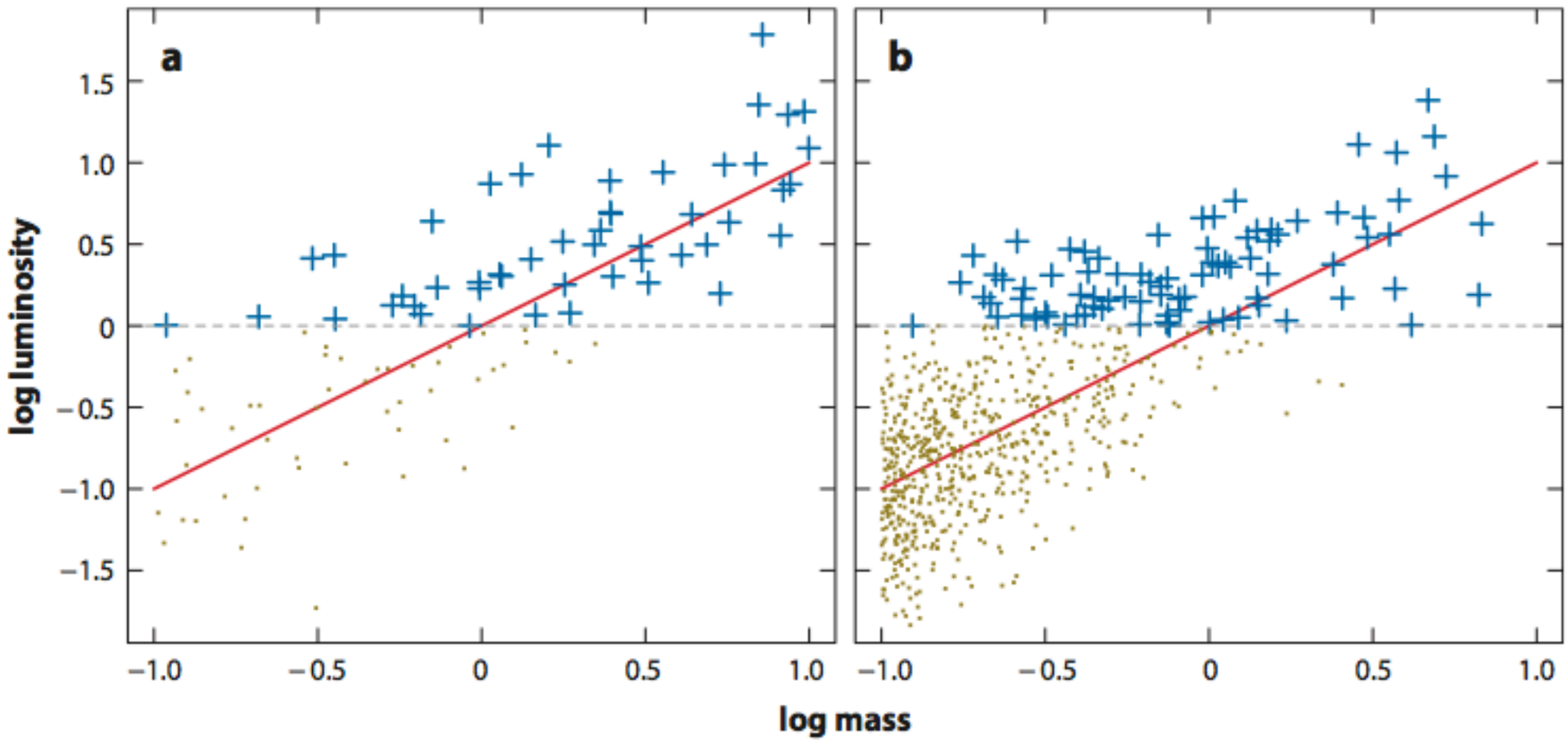

Figure 5

Diagrams illustrating generically how the distribution of observed scaling relation data (*blue crosses*) do not reflect the underlying scaling law (*red line*) due to selection effects (e.g., a luminosity threshold; *dashed gray line*). Dark yellow dots indicate undetected sources. (*a*) An unphysical case in which cluster log masses are uniformly distributed; (*b*) a case with a more realistic, steeper mass function than in panel *a* (normalized to produce roughly the same number at high masses). The steepness of the mass function has a clear effect on the degree of bias in the detected sample. To recover the correct scaling relation, an analysis must account for both the selection function of the data and the underlying mass function of the cluster population. Adapted from Mantz et al. (2010a).

Scaling relation pitfalls

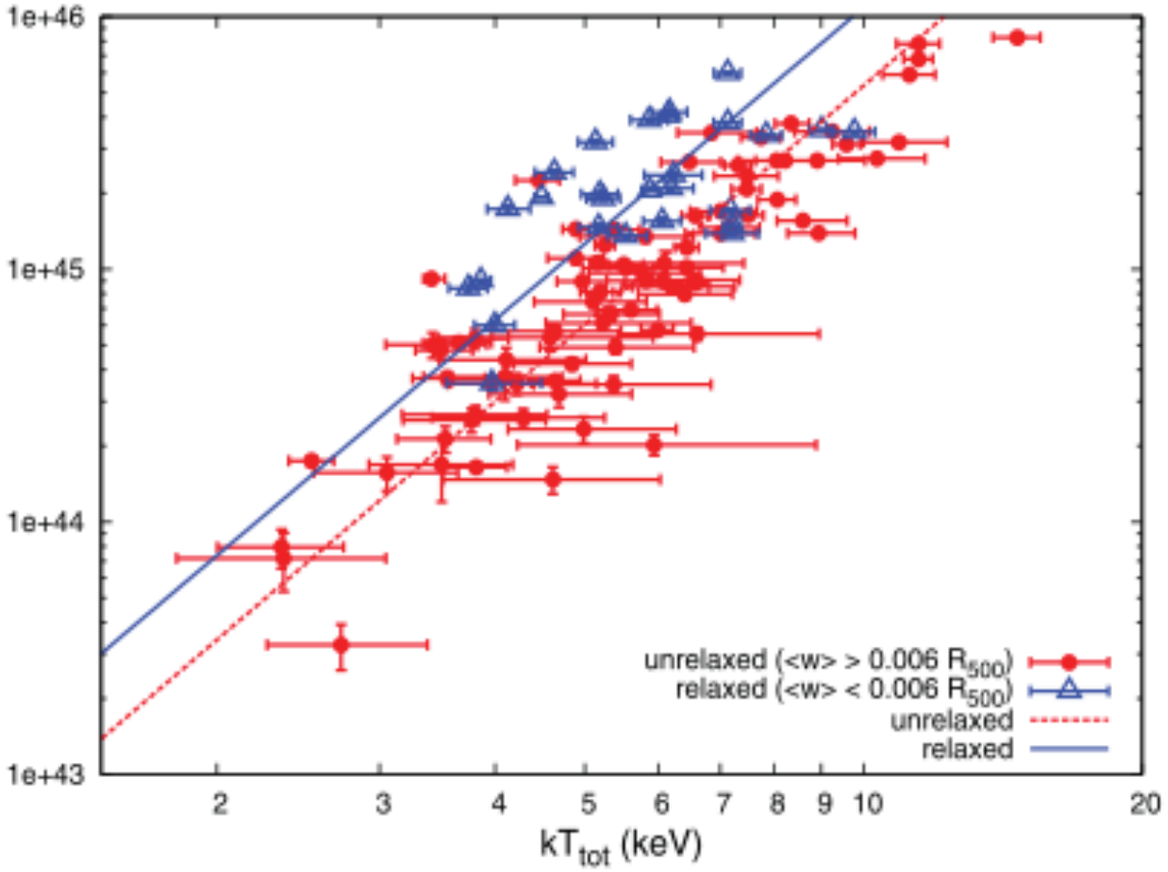

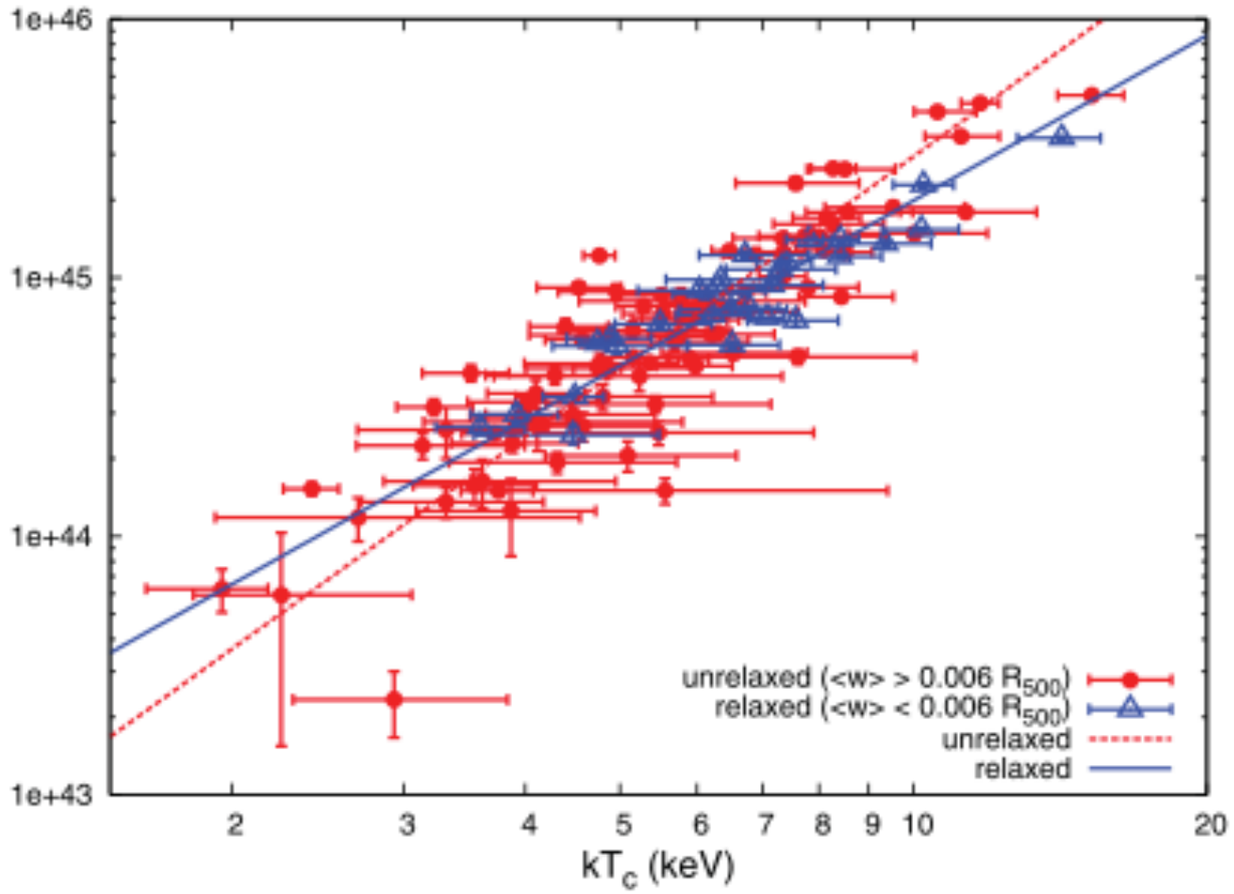

L-T relation for relaxed and non-relaxed clusters, before and after removing the core component (from Maughan et al. 2012)

X-ray emission from clusters

Thermal Bremsstahlung

$$\epsilon(\nu) = \frac{16\, e^6}{3\, m_e\, c^2}\left(\frac{2\pi}{3 m_e\, k_B T_X}\right)^{1/2} n_e n_i\, Z^2\, g_{ff}(Z, T_X, \nu)\, \exp\left(\frac{-h\nu}{k_B T_X}\right),$$

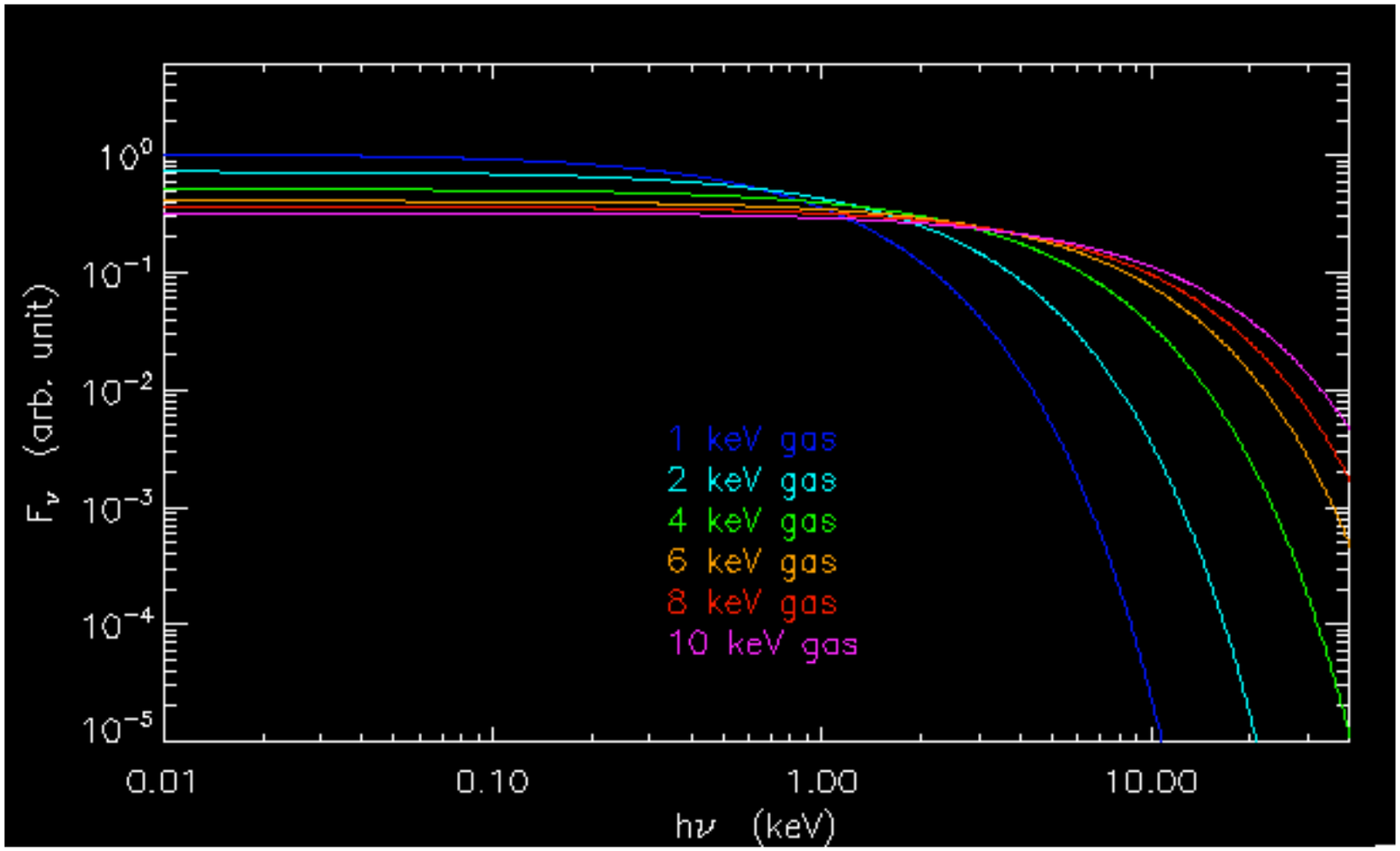

X-ray emission from clusters

Thermal Bremsstahlung

$$\epsilon(\nu) = \frac{16\ e^6}{3\ m_e\ c^2}\left(\frac{2\pi}{3 m_e\ k_B T_X}\right)^{1/2} n_e n_i\ Z^2\ g_{ff}(Z, T_X, \nu)\ \exp\left(\frac{-h\nu}{k_B T_X}\right),$$

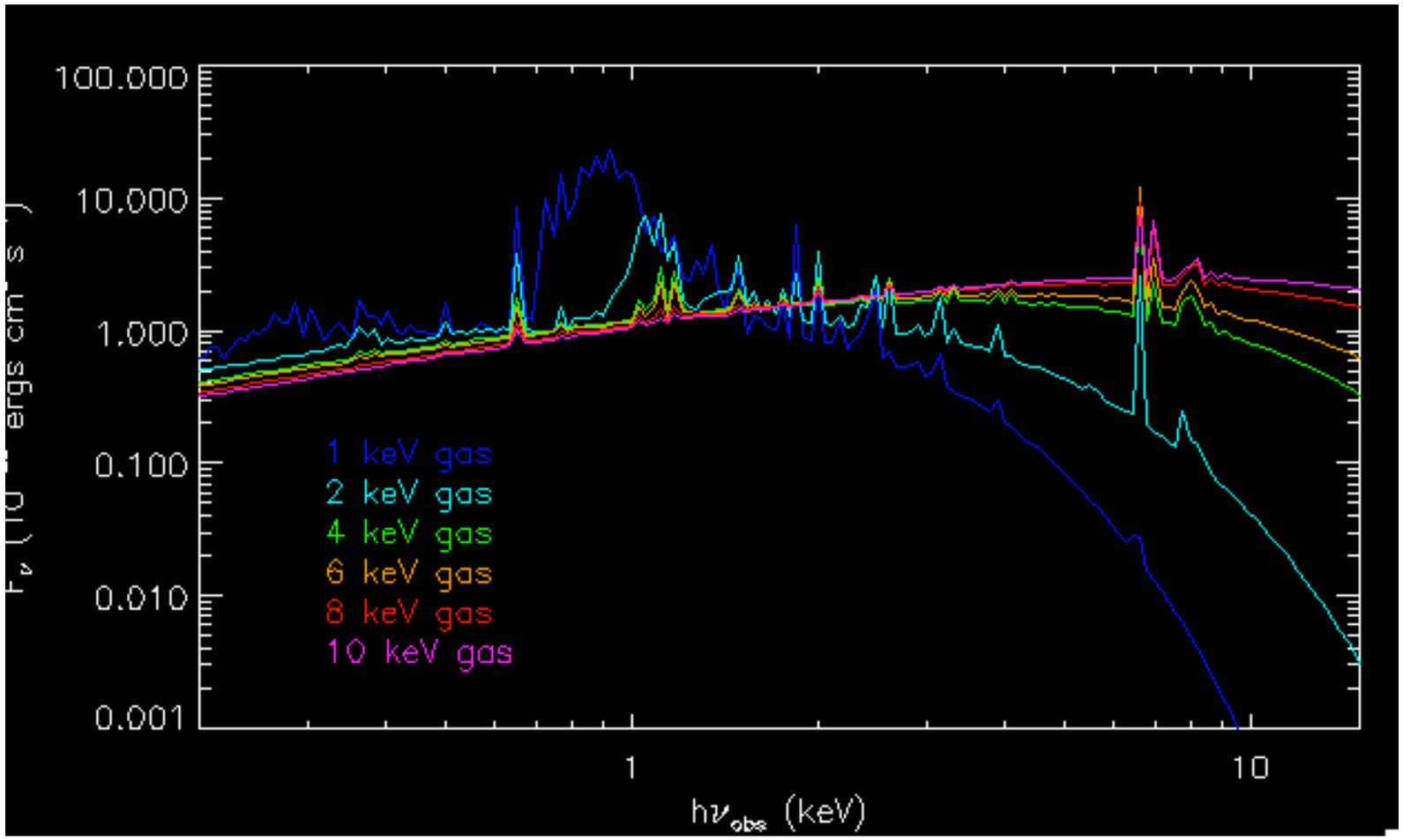

X-ray cluster profile

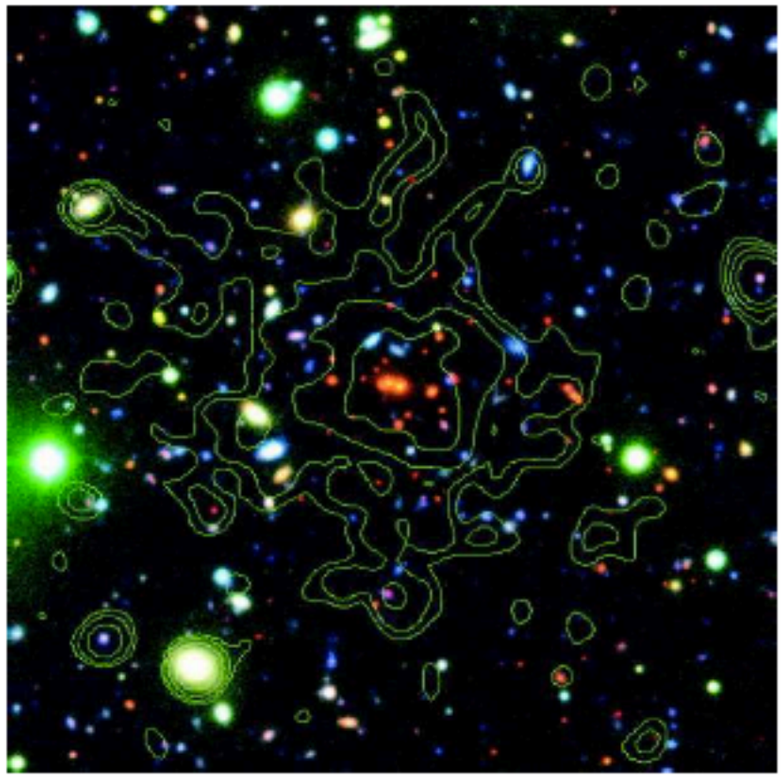

Fig. 3. – Image of the cluster RDCS 1252.9-2927 at $z = 1.24$. Contours of the *Chandra* emission are overlaid on a composite VLT image. Figure from [24]

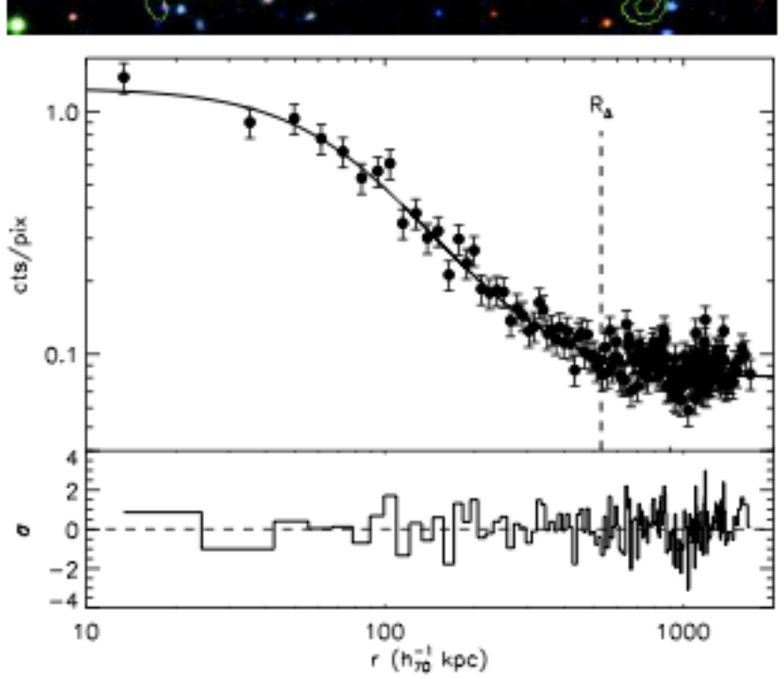

Fig. 4. – Surface brightness profile of RDCS 1252.9-2927 measured with *Chandra* (data points), with best-fit model (solid line) and residuals. Figure from [24]

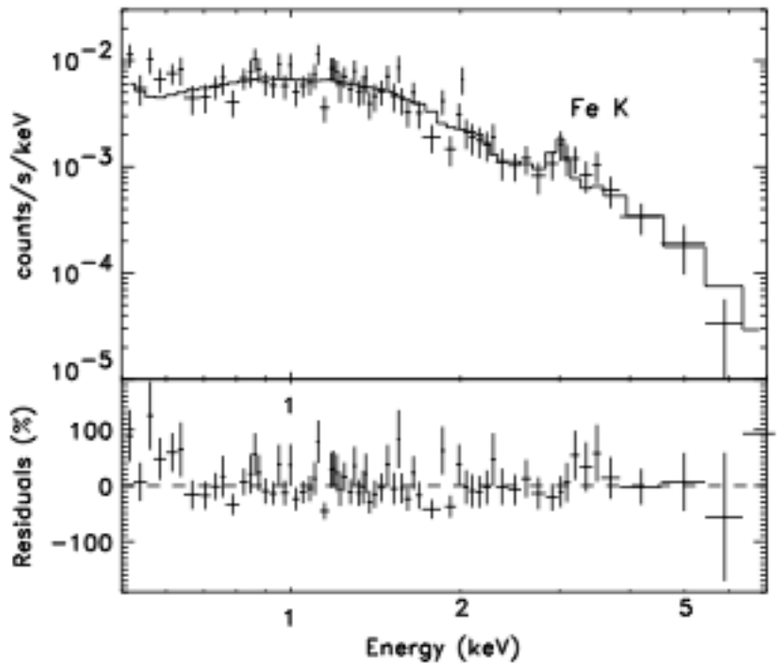

Fig. 5. – X-ray spectrum of RDCS 1252.9-2927 (data points) and best-fit thermal model (solid line) from *XMM-Newton* observation. Note the redshifted Iron line. Figure from [24]

Example: X-ray derived mass

A) X-ray Image

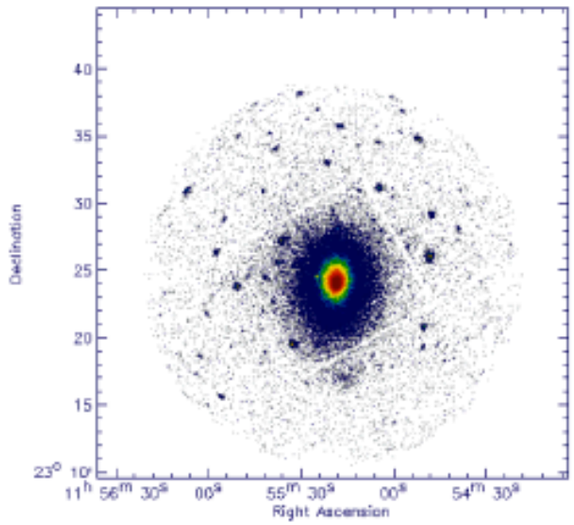

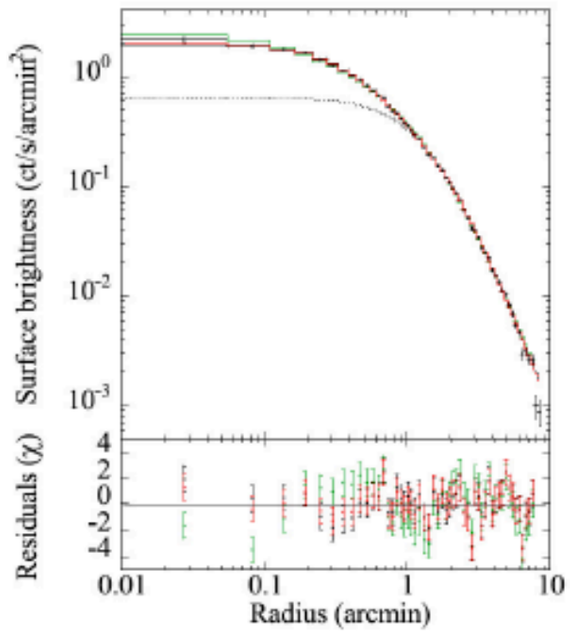

B) Surface Brightness Profile

β -model profile

C) Temperature Profile

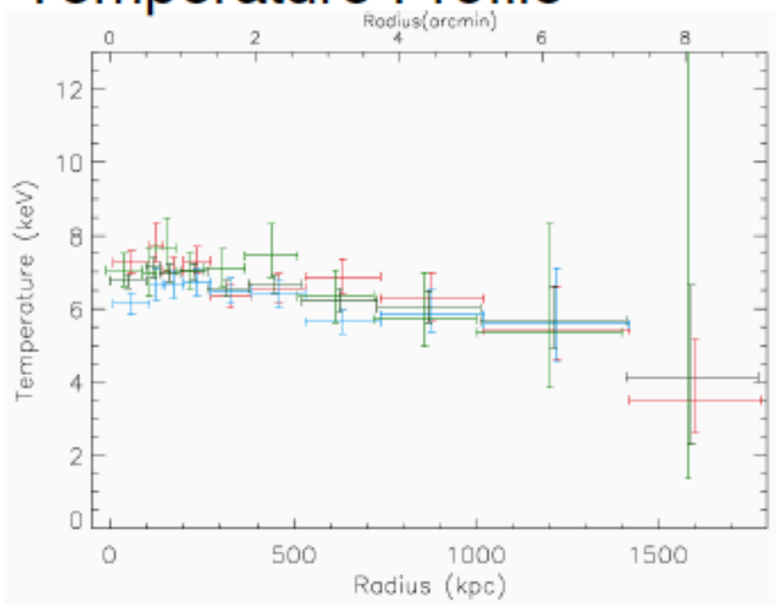

Source: Pratt & Arnaud 2002

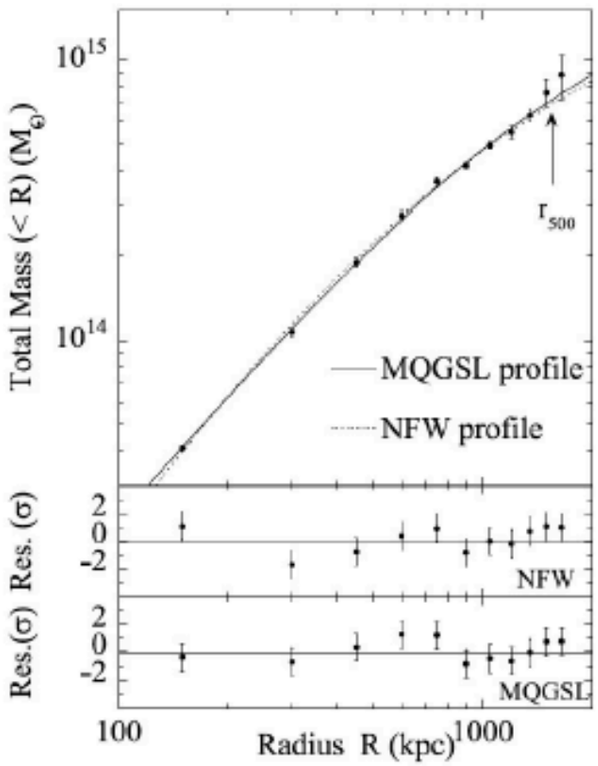

D) Mass Profile

NFW profile

$M_{200}=6.5\times10^{14}\ M_{sun}$

Mass from density & temp. profiles

Total mass from X-ray is determined by assuming
1. spherical symmetry, 2. hydrostatic equilibrium

$$\frac{d\Phi}{dr} = \frac{G M_{tot}(<r)}{r^2} = -\frac{1}{\rho_{gas}} \frac{dP_{gas}}{dr}$$

$$M_{tot}(<r) = -\frac{kT_{gas}(r)\ r}{G\mu m_p} \left(\frac{\partial \ln n_{gas}}{\partial \ln r} + \frac{\partial \ln T_{gas}}{\partial \ln r} \right)$$

$$M_{tot}(<r) \propto r \times T_{gas}(r) \times (-\alpha_n - \alpha_T)$$

α_n~ **-2/-2.4** α_T~ **0/-0.8**

X-ray temperature profile

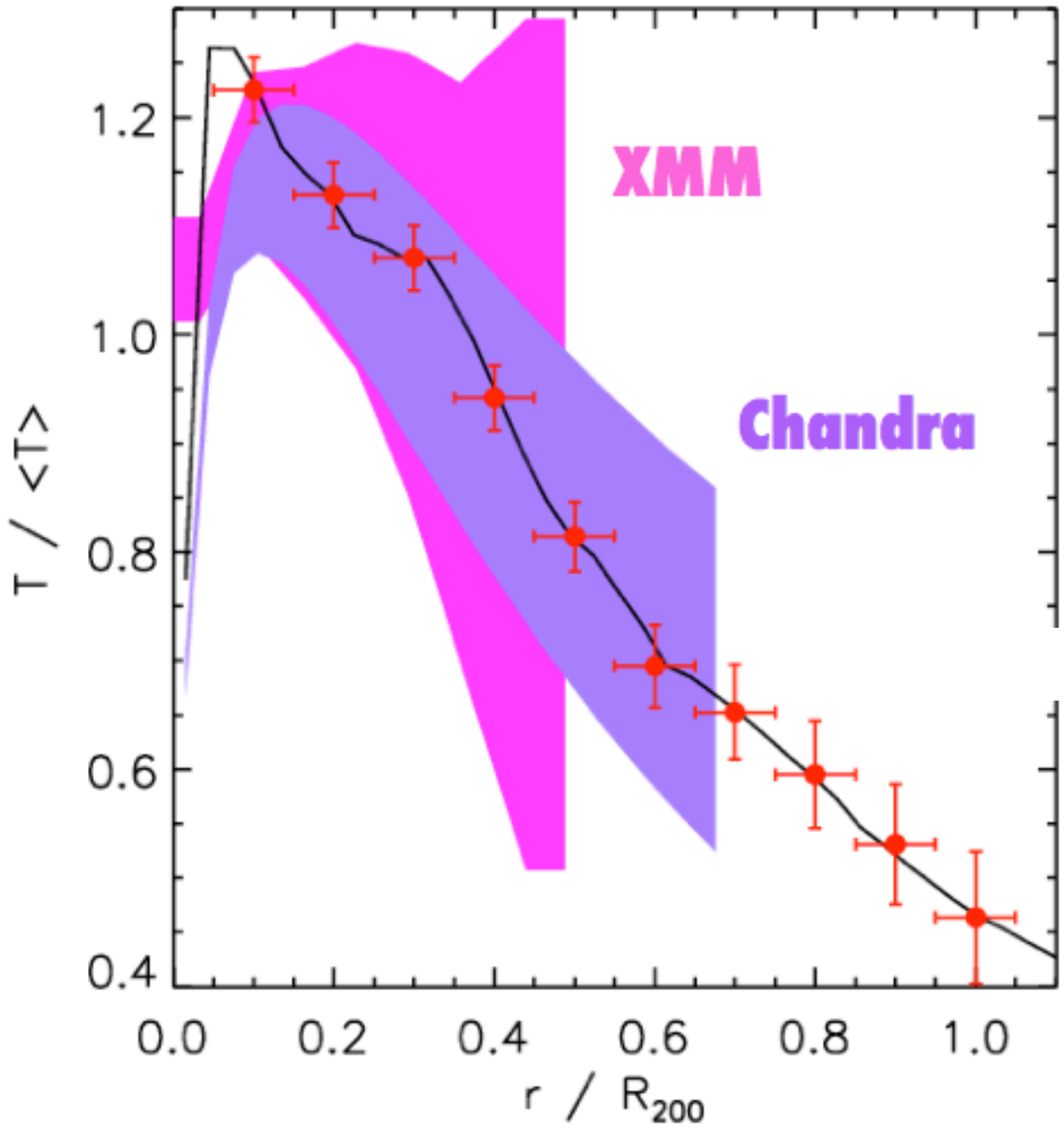

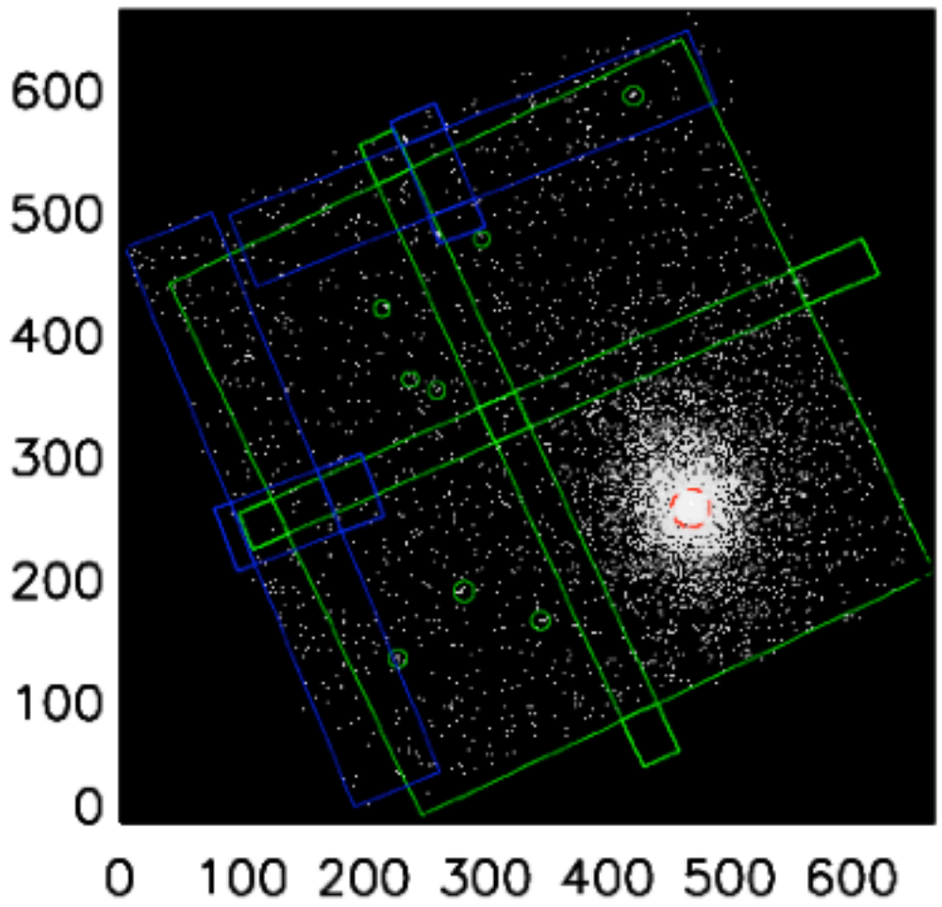

A1689: ~30000 photons in 10 ks

Tx in the cluster outskirts

Perseus cluster with Suzaku satellite (Simionescu et al. 2011)

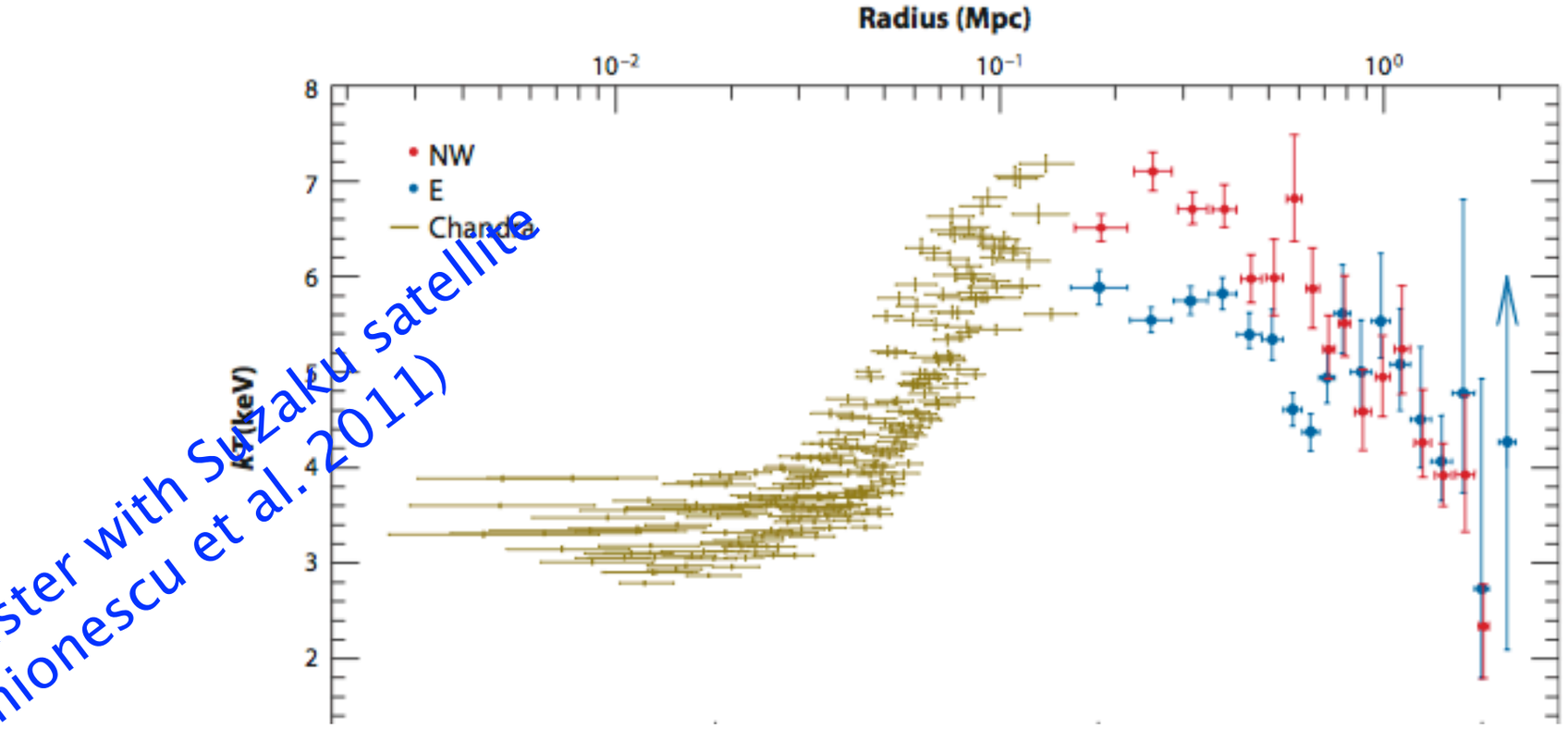

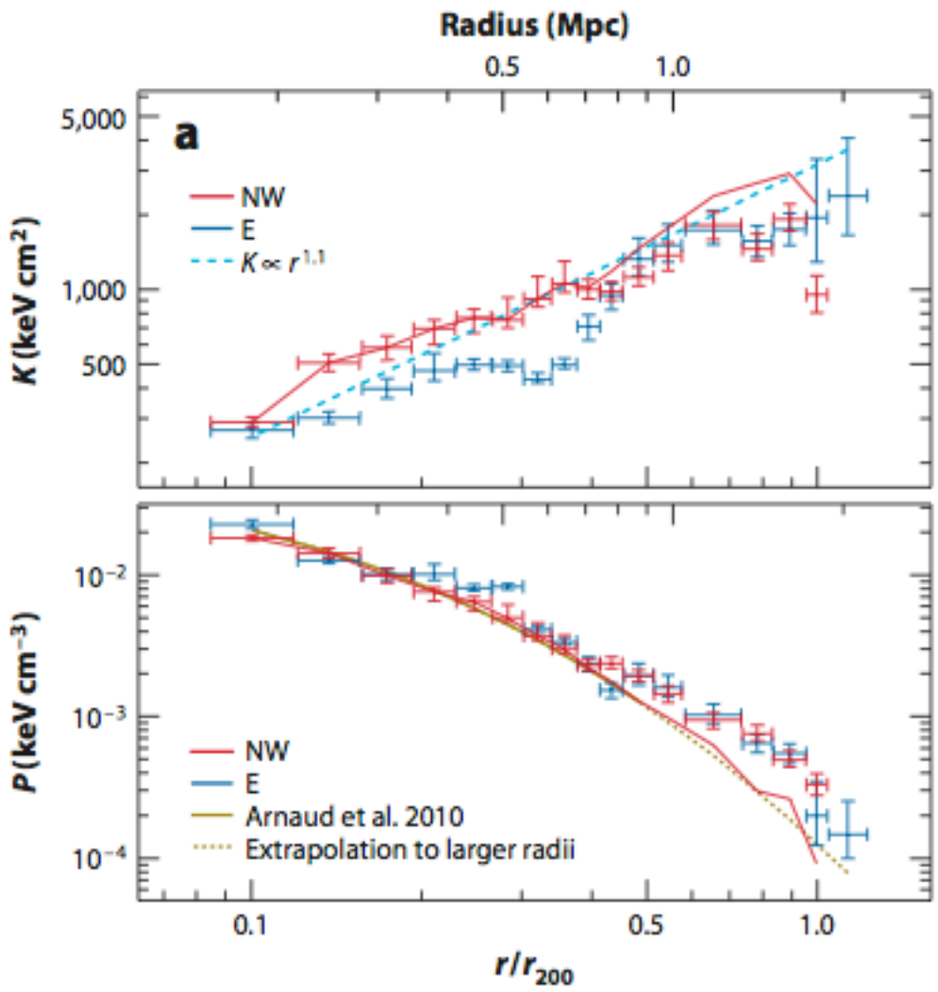

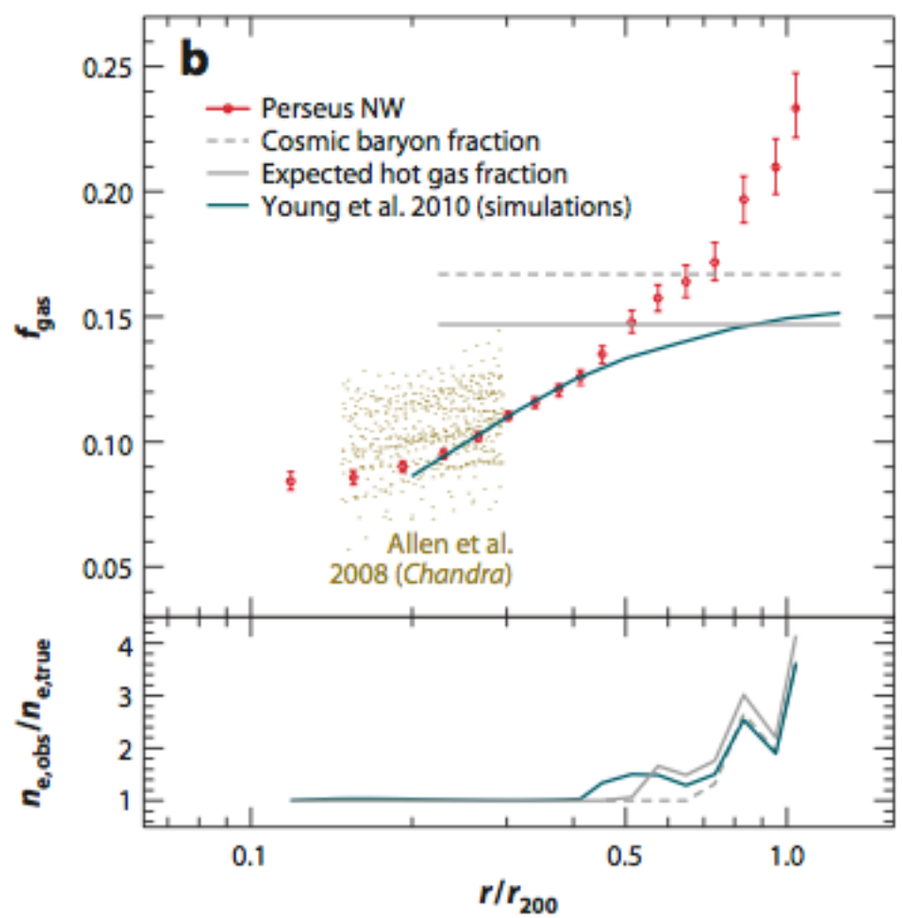

ICM entropy

$$K = T_e \, n_e^{-2/3}$$

Entropy is a fundamental indicator of heating/cooling in the ICM (it remains unchanged during adiabatic processes)

This simply follows from the adiabatic index:
$K = P \, \rho^{-5/3}$

The classic definition of entropy for a monatomic ideal gas is then:
$s = \ln K^{3/2} + \text{const}$

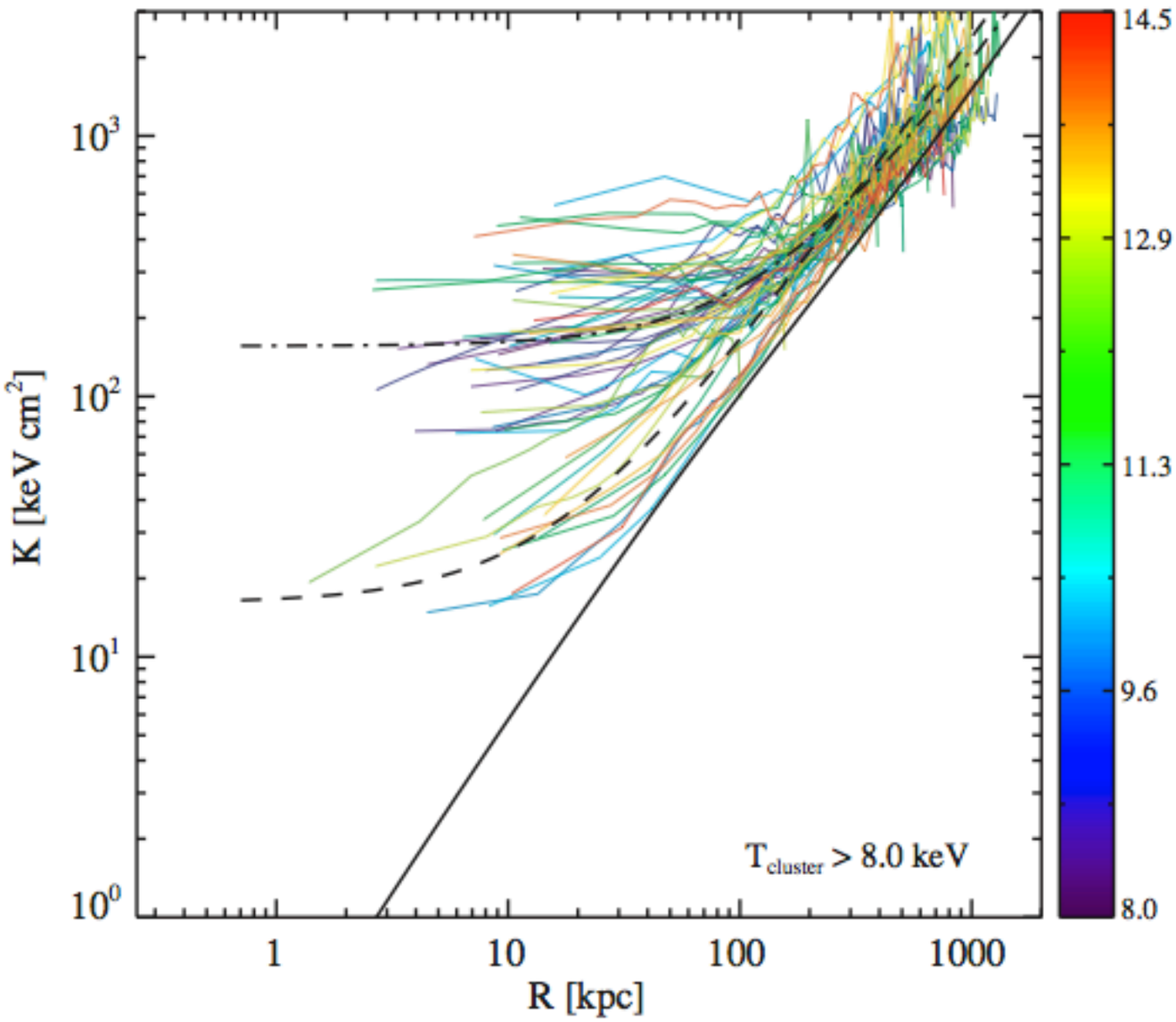

ICM structures in X-rays

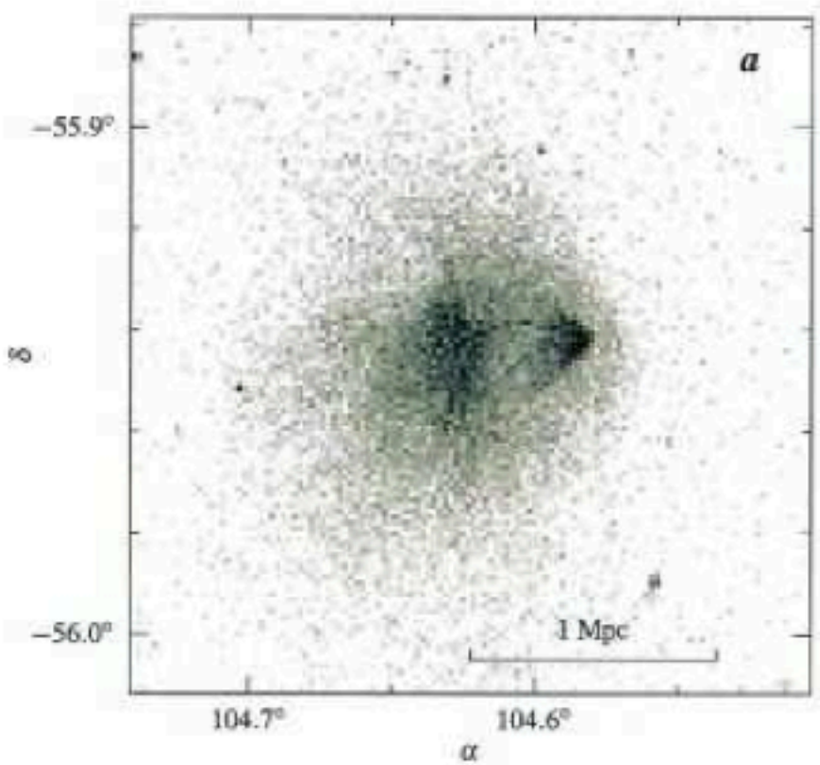

Fig. 8. – *Chandra* image of 1E0657-56. Note the "bullet" apparently just exiting the cluster core and moving westward. The bullet is preceded by an X-ray brightness edge that resembles a bow shock. Figure from [38]

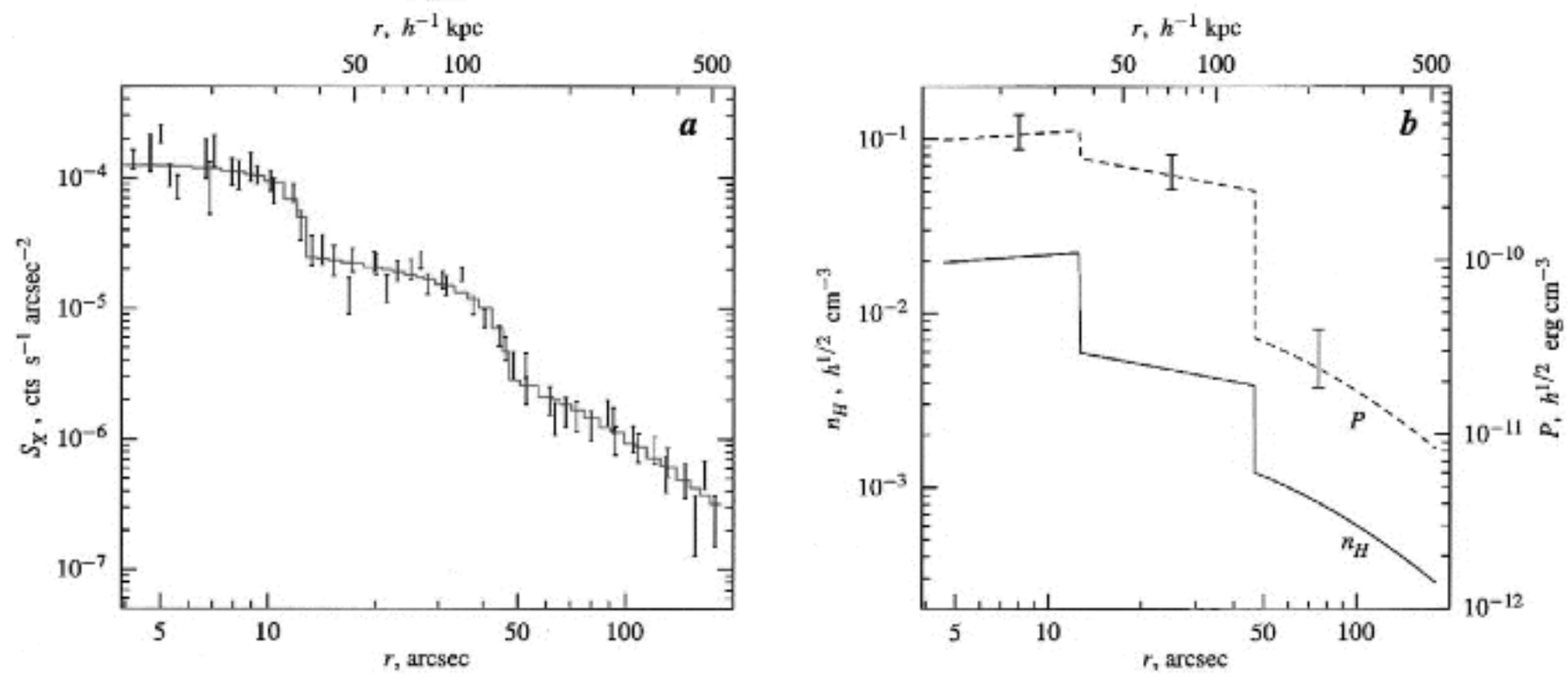

Fig. 9. – Surface brightness profile in a 120° sector centered on the bullet and directed westward (Left) and corresponding temperature and pressure profile (right). The first edge is a cold front while the second is a shock. Figure from [38]

ICM structures in X-rays

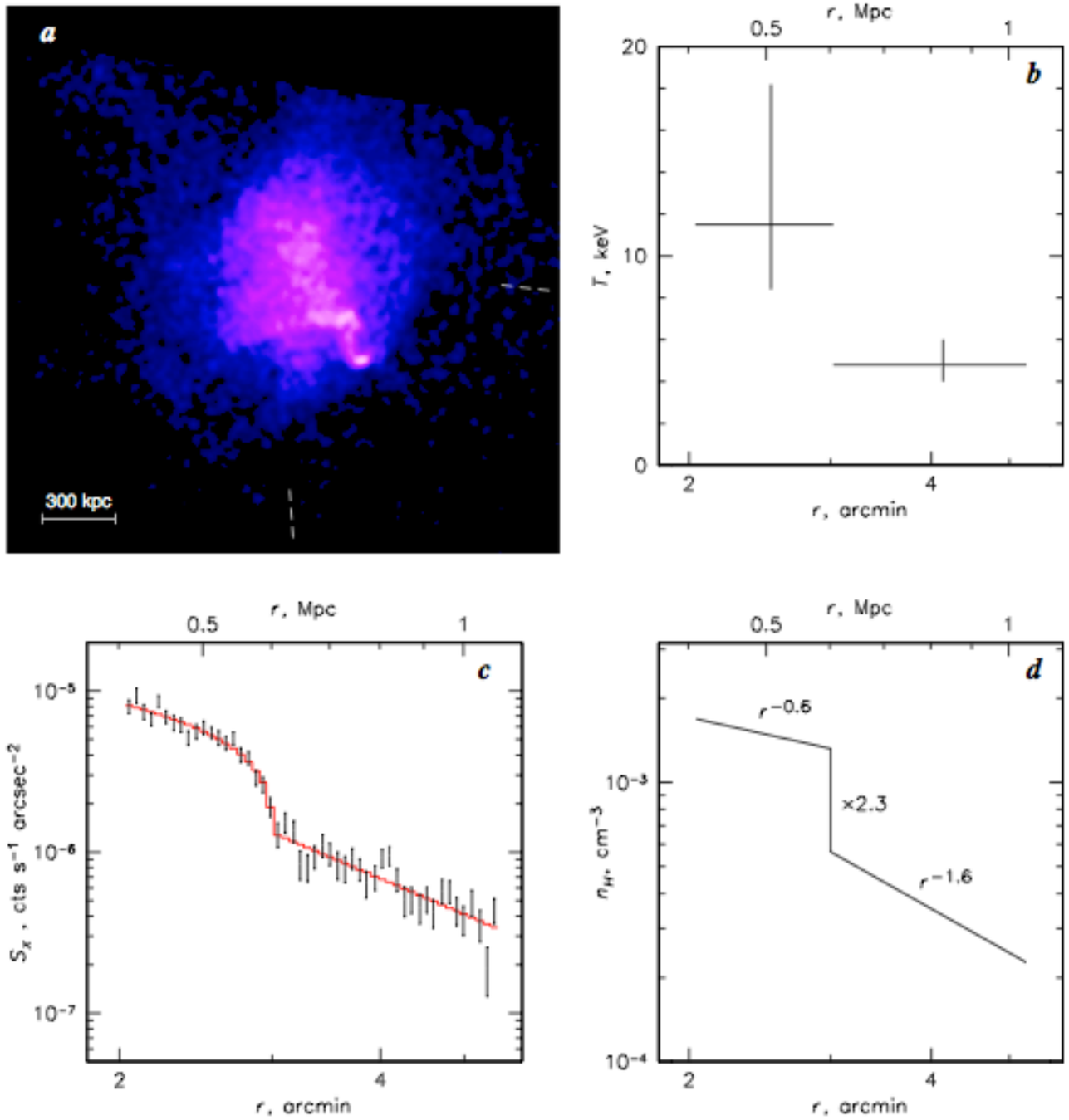

Fig. 33. Shock front in A520. (*a*) A *Chandra* image (slightly smoothed) with point sources removed. The bow shock is a faint blue edge southwest of the bright irregular remnant of a dense core. White dashed lines mark a sector used for radial X-ray brightness and projected temperature profiles across the shock (panels *b*,*c*). The profiles are extracted excluding the core remnant. (*d*) A three-dimensional model fit to the brightness profile; its projection is shown as a red line in panel (*c*). (Reproduced from M05.)

Gas sloshing & cold fronts

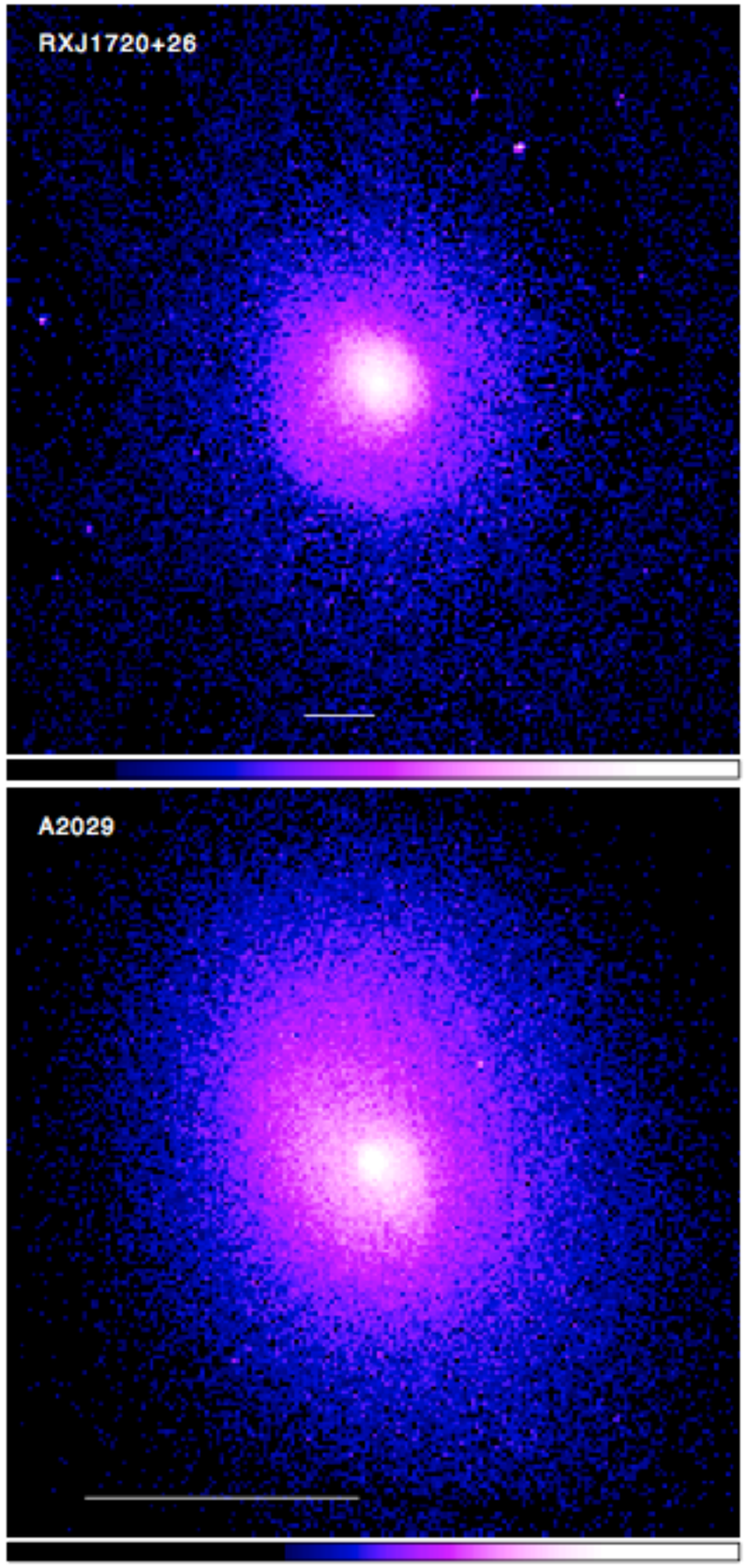

Fig. 16. The origin of cold fronts in the dense cluster cores.

The Sunyaev-Zel'dovich (SZ) effect

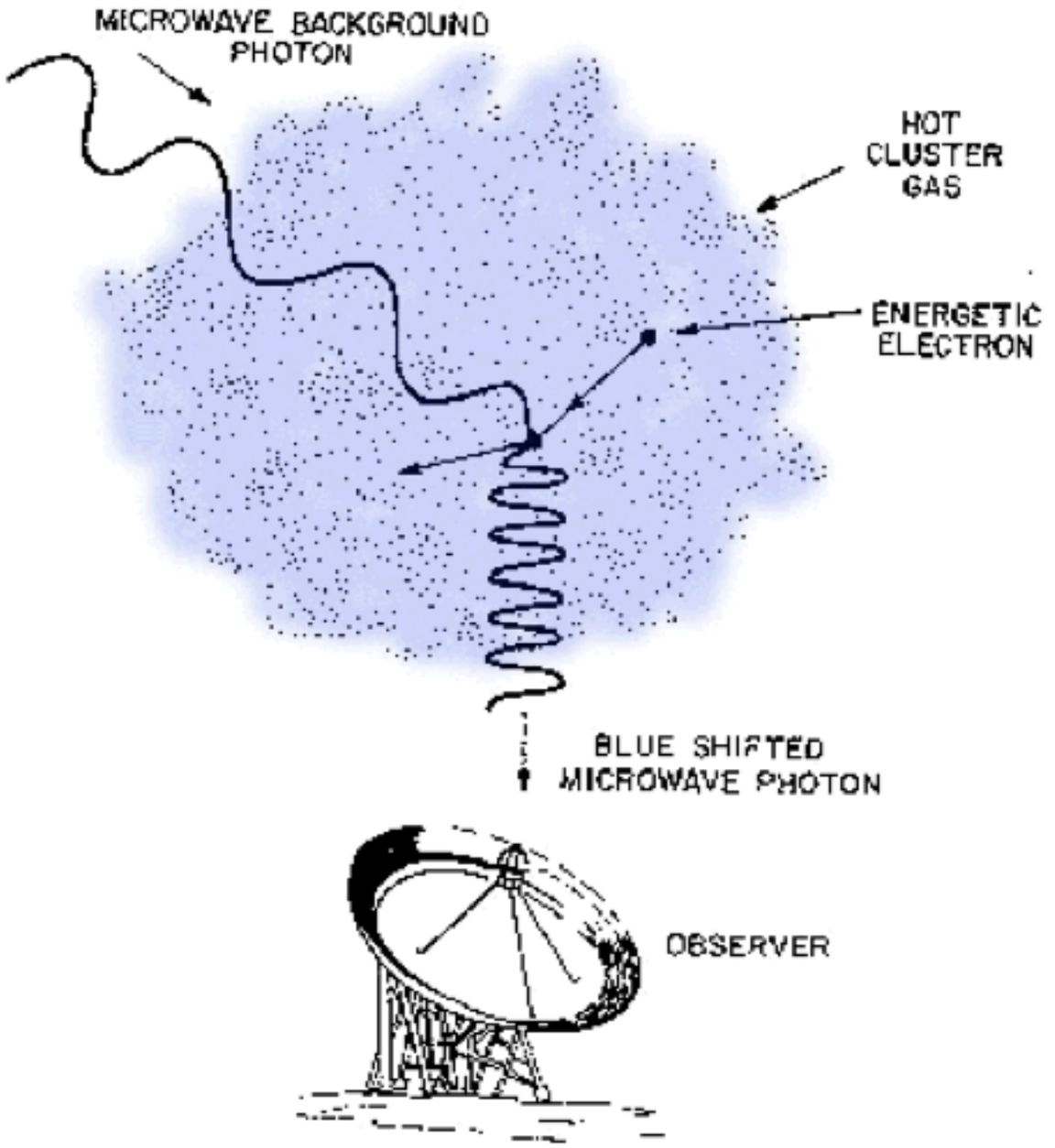

Source: http://astro.uchicago.edu/sza/primer.html

The Sunyaev-Zel'dovich (SZ) effect

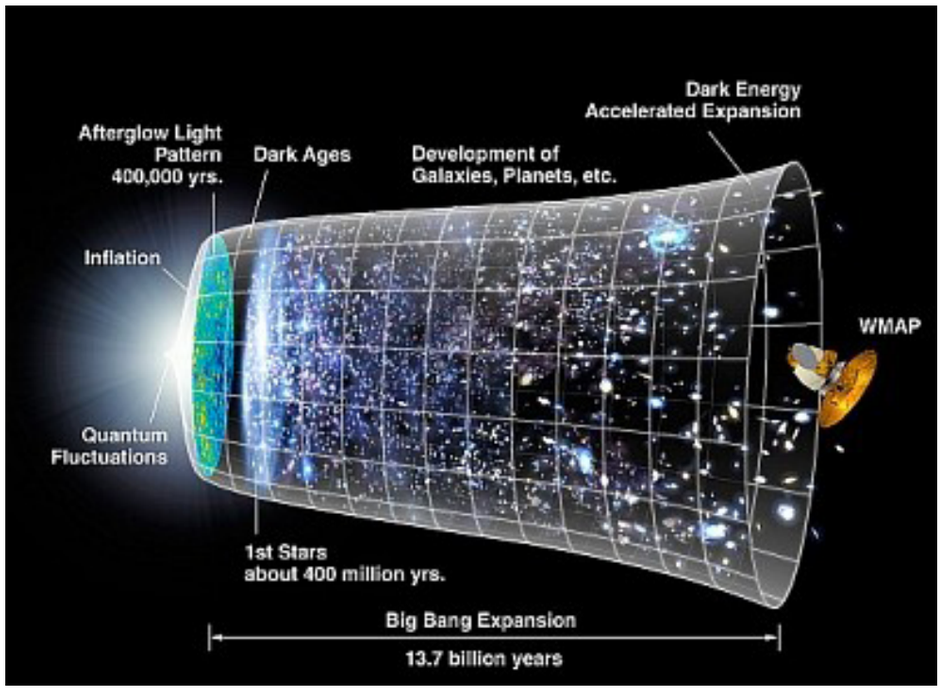

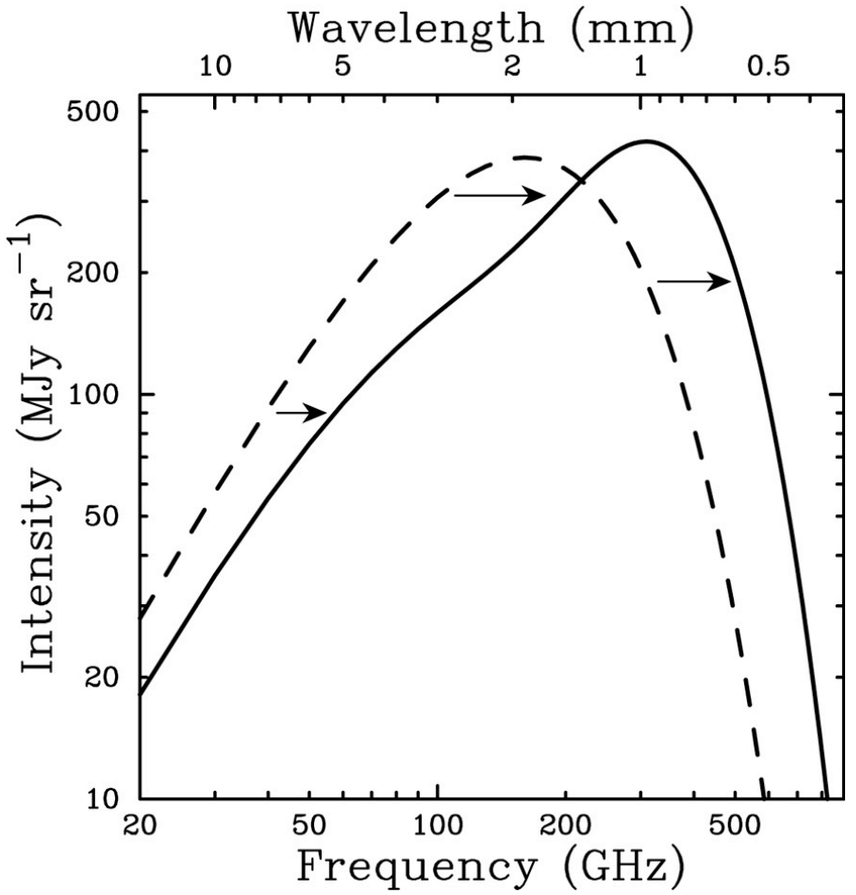

1-2% of the CMB photons traversing galaxy clusters are inverse Compton scattered to higher energy

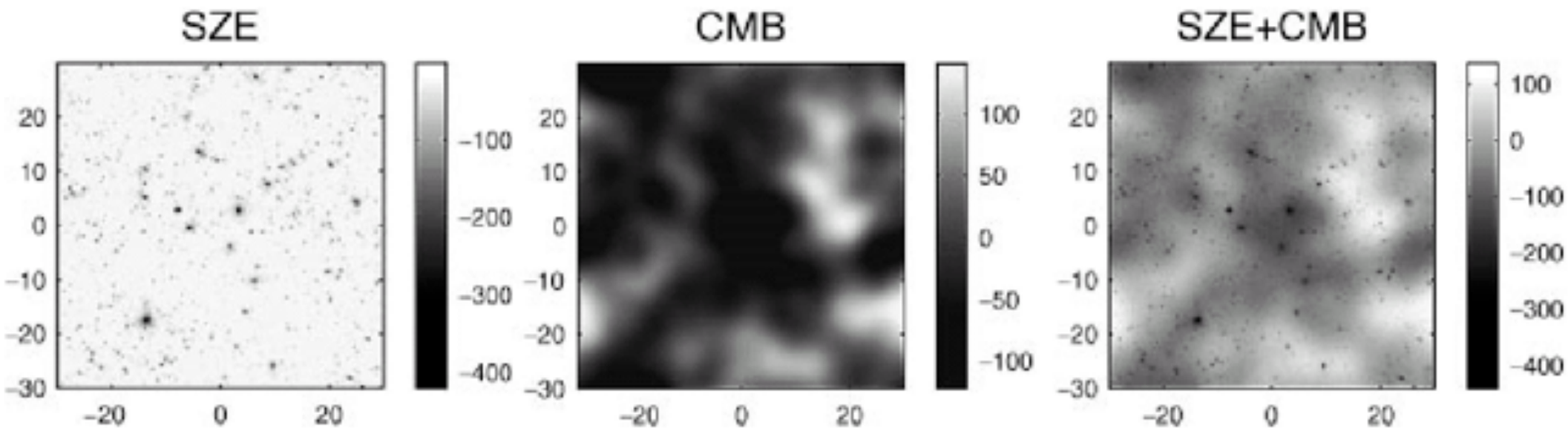

Compton scattering

a photon of initial wavelength λ and energy hν deflected off a stationary free electron by an angle θ exhibits a wavelength gain and energy loss after scattering (S) of the form (energy & momentum conservation):

$$\lambda_S - \lambda = \lambda_C (1 - \cos\theta)$$

$$h\nu_S = \frac{h\nu}{1 + \lambda_C (\nu/c)(1 - \cos\theta)} \qquad \text{(e1)}$$

with Compton wavelength:

$$\lambda_C = \frac{h}{m_e c} = 2.43 \times 10^{-12} m = 2.43 pm = (511 keV/hc)^{-1}$$

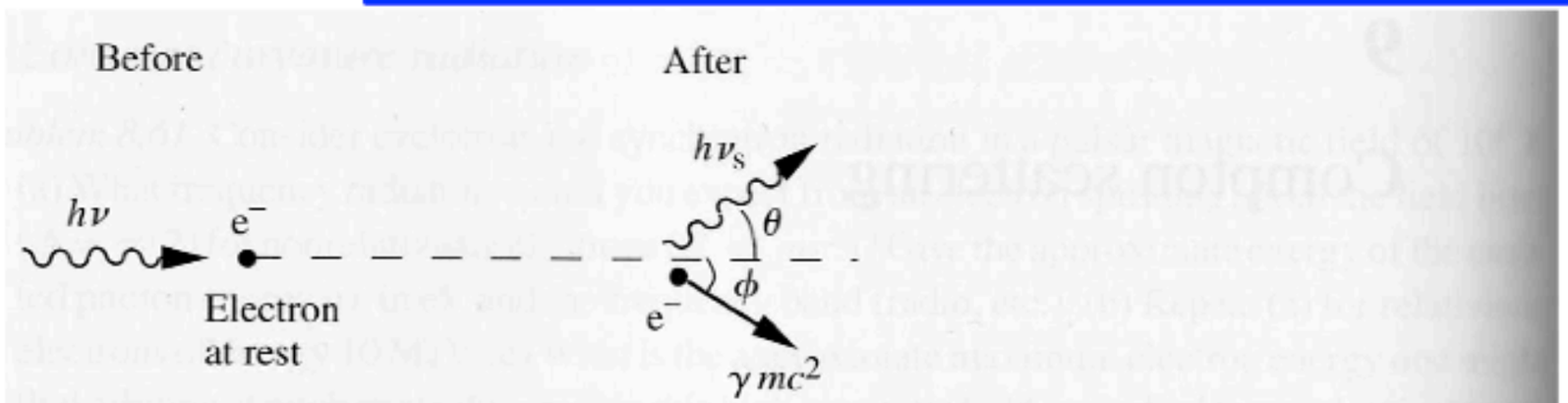

Figure 9.1. Normal Compton scattering. A photon scatters off of a stationary free (unbound) electron, giving part of its energy to the electron. The energy of the scattered photon is a function of the photon scattering angle θ.

Source: ‚Astrophysics Processes', Bradt 2008

Inverse Compton scattering

the inverse effect, i.e. the scattered photon gains energy, can be calculated from the normal Compton effect via appropriate Lorentz transformations in and out of the electron's system of reference

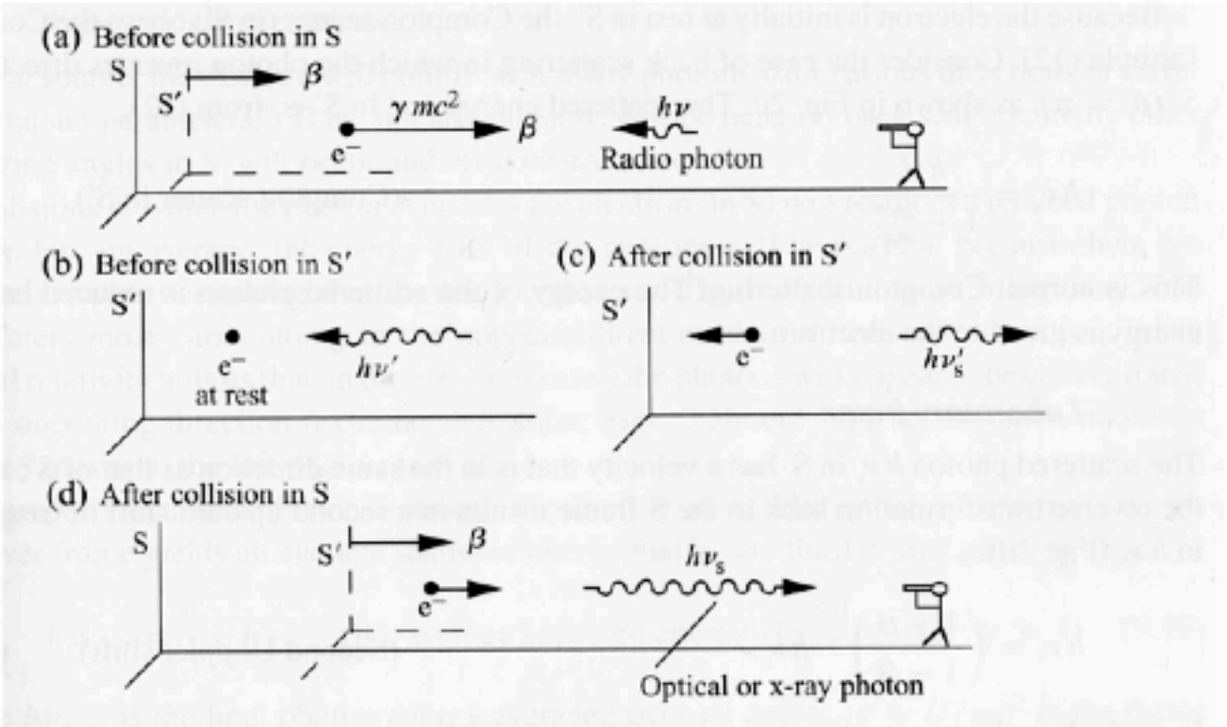

Figure 9.2. Inverse Compton effect for head-on interaction. (a) S frame before the scatter. A highly relativistic electron moves to the right and is about to collide with a left-moving, low-energy (radio) photon of energy $h\nu$. The S′ frame moves with the electron. (b) S′ frame before scatter. The electron is at rest, and so the scatter becomes a normal Compton scatter. The incident photon in S′ has been Doppler shifted to higher energy $h\nu'$ because of the motion of this frame relative to S. (c) S′ frame after scatter. The photon, having been backscattered with energy $h\nu'_s$, moves to the right with slightly less energy. (d) S frame after scatter. The scattered photon has a much higher energy $h\nu_s \gg h\nu'_s$ owing to the transformation back to frame S.

Source: ‚Astrophysics Processes', Bradt 2008

S: observers frame, in which electron has velocity

$$\beta = v/c$$

and Lorentz factor

$$\gamma = \left(1 - \frac{v^2}{c^2}\right)^{-1/2}$$

S´: electron rest frame before scattering

Idea:

1) transform from S to S´
2) observe normal Compton scattering event in S´
3) transform back to S

Inverse Compton scattering

For ICM:

$$E_{kin} \approx 5-10\text{keV} \rightarrow \gamma \approx 1.01-1.02 \quad \text{and} \quad \beta \approx 0.1-0.2$$

for β~0.15 (T~5keV): $\sqrt{\frac{1+\beta}{1-\beta}} \approx \sqrt{(1+\beta)^2} \approx (1+\beta)$

maximum fractional energy increase of single IC back-scattered photon with T~5 keV electron:

$$h\nu_s \approx (1+\beta)^2 \frac{h\nu}{1+2\lambda_C \frac{\nu}{c}(1+\beta)} \approx (1+\beta)^2 h\nu \approx 1.3\, h\nu$$

the Sunyaev-Zeldovich Effect is the distortion of the blackbody CMB spectrum owing to Inverse Compton scattering of the CMB photons with the energetic ICM electrons

average fractional IC photon net energy gain from a 5keV plasma from single scattering events, averaged over all collision angles and electron speeds:

$$\left\langle \frac{\Delta\nu}{\nu} \right\rangle \approx \frac{4kT_e}{m_e c^2} \approx 0.04 \approx 4\%$$

Spectrum of the SZ effect

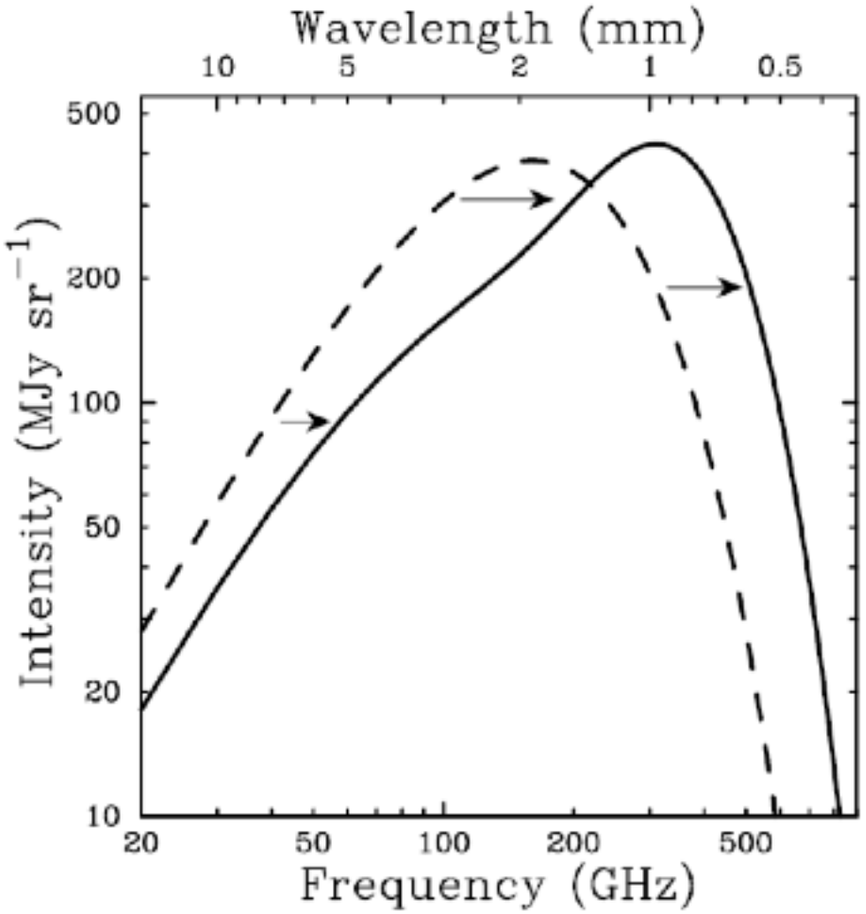

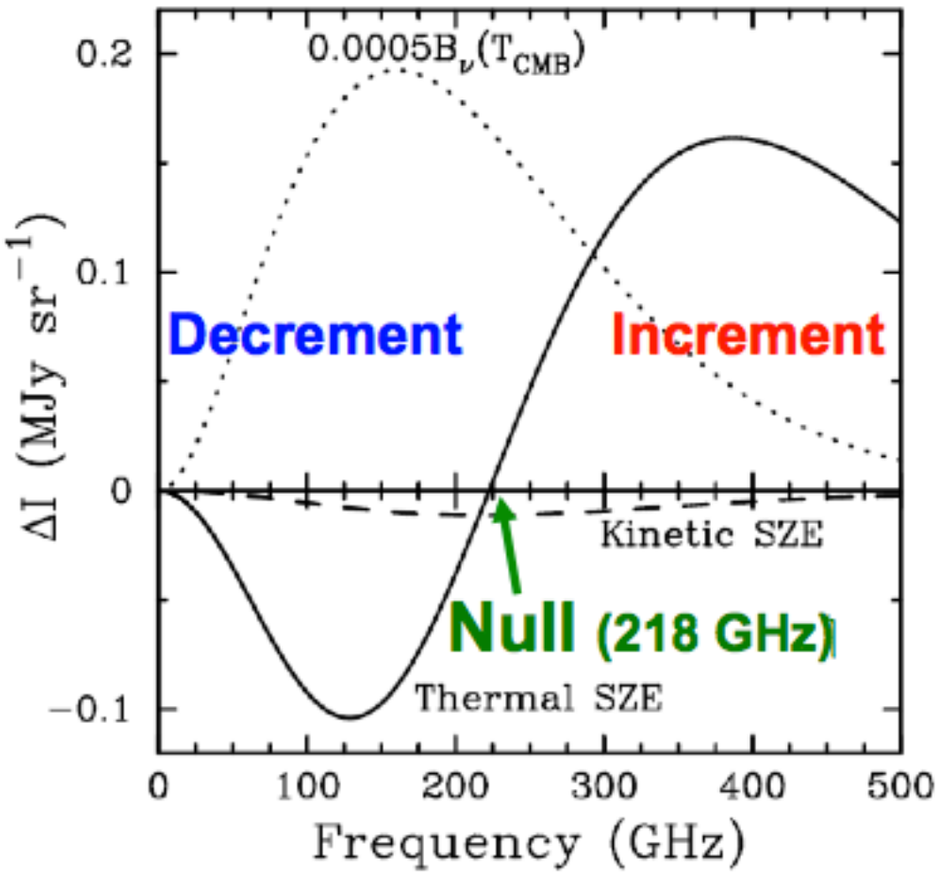

decrement in Rayleigh-Jeans part: $\Delta I(\nu) = -2\, y\, I(\nu)$

Compton-y parameter: $y \equiv \frac{\sigma_{\rm T}\, k_{\rm B}}{m_{\rm e}\, c^2} \int T_{\rm e}\, n_{\rm e}\, dl$

integrated effect: $Y = \int y\, dA \propto n_{\rm e}\, T\, dV \propto E_{\rm thermal}$

Source: Carlstrom et al., 2002

Properties of the SZ effect

Thermal SZE is a small (<1 mK) distortion in the CMB caused by inverse Compton scattering of the CMB photons

$$\frac{\Delta T}{T_{\rm CMB}} = g(x) \int n_e(l) \, \frac{k_{\rm B} T_e(l)}{m_e c^2} \, dl$$

Total cluster flux density is independent of redshift!

$$\Delta S_\nu = \int \Delta I_\nu \, d\Omega \propto \frac{\int n_e T_e \, dV}{D_{\rm A}^2} \propto \frac{f_{\rm gas} M_{\rm tot} T_e}{D_{\rm A}^2}$$

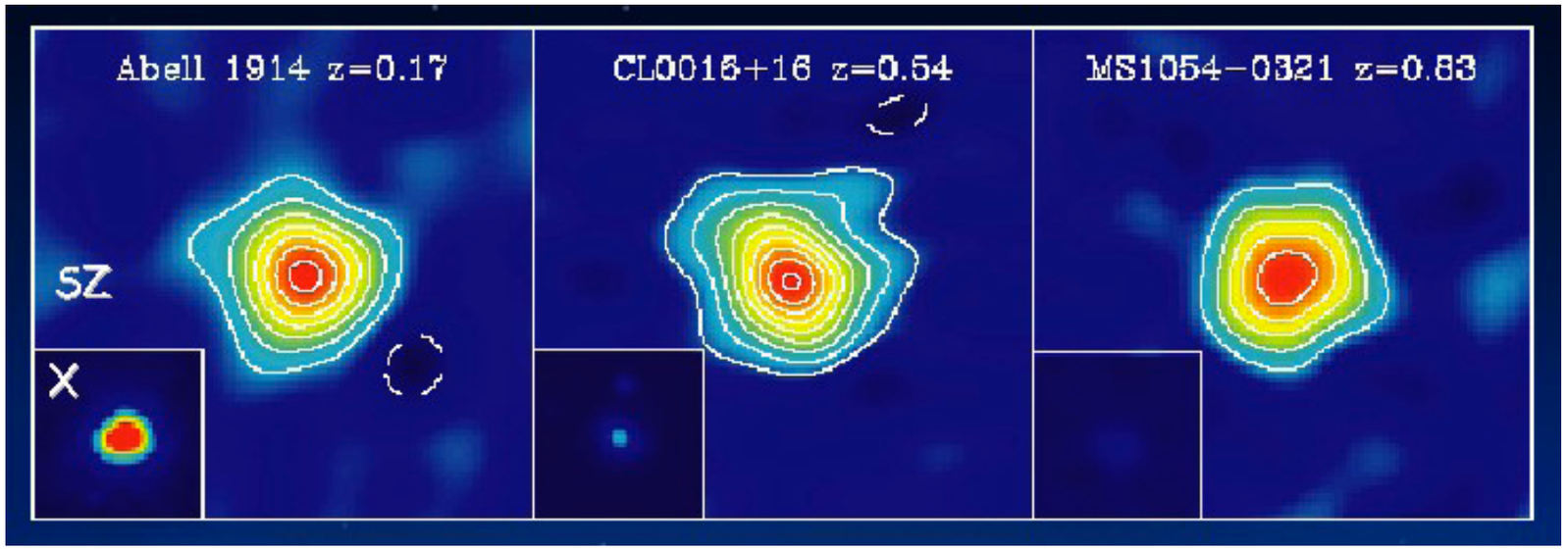

Kinematic SZ effect (kSZ)

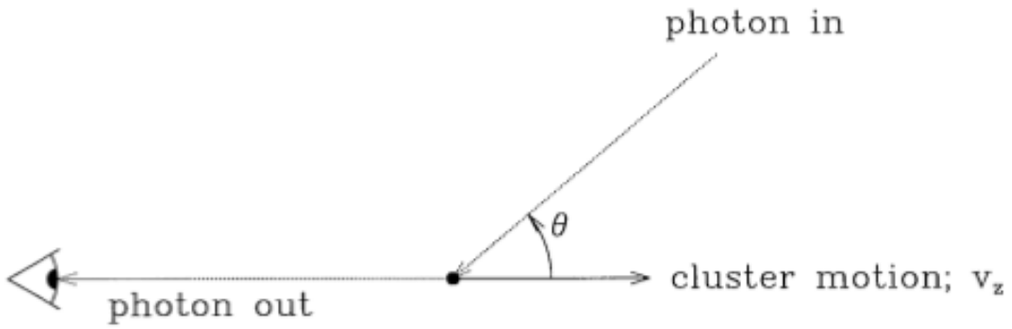

$$\frac{\Delta T_{SZE}}{T_{CMB}} = -\tau_e \left(\frac{v_{pec}}{c}\right),$$

Net change in photon energy due to peculiar motion of the cluster in the CMB rest frame (Doppler effect)

Sum of kSZ signal in many clusters will be zero.

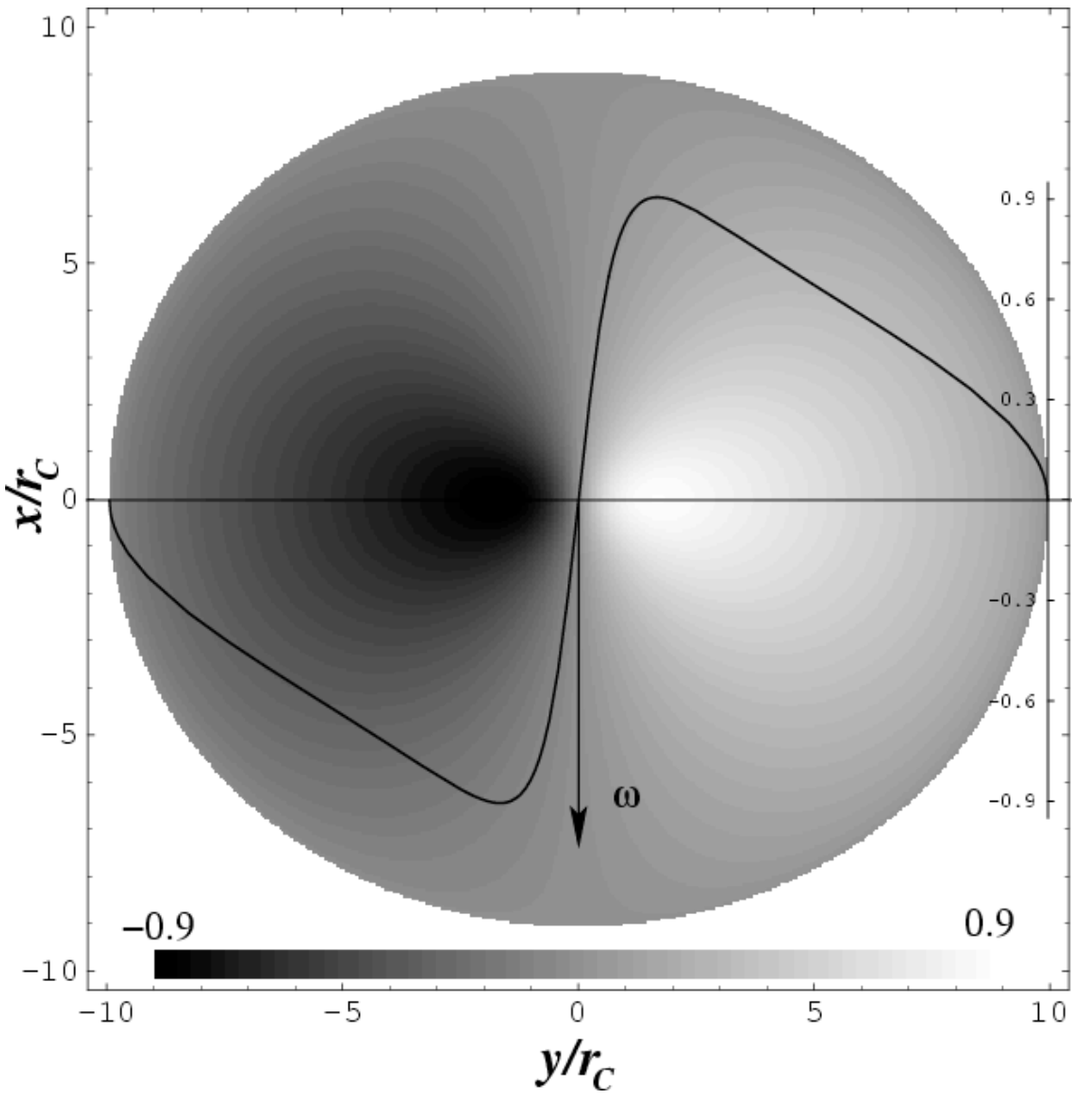

Also: cluster rotation!
(Chluba & Mannheim 2002)

SZ: A new window

a simulated massive galaxy cluster at z=0

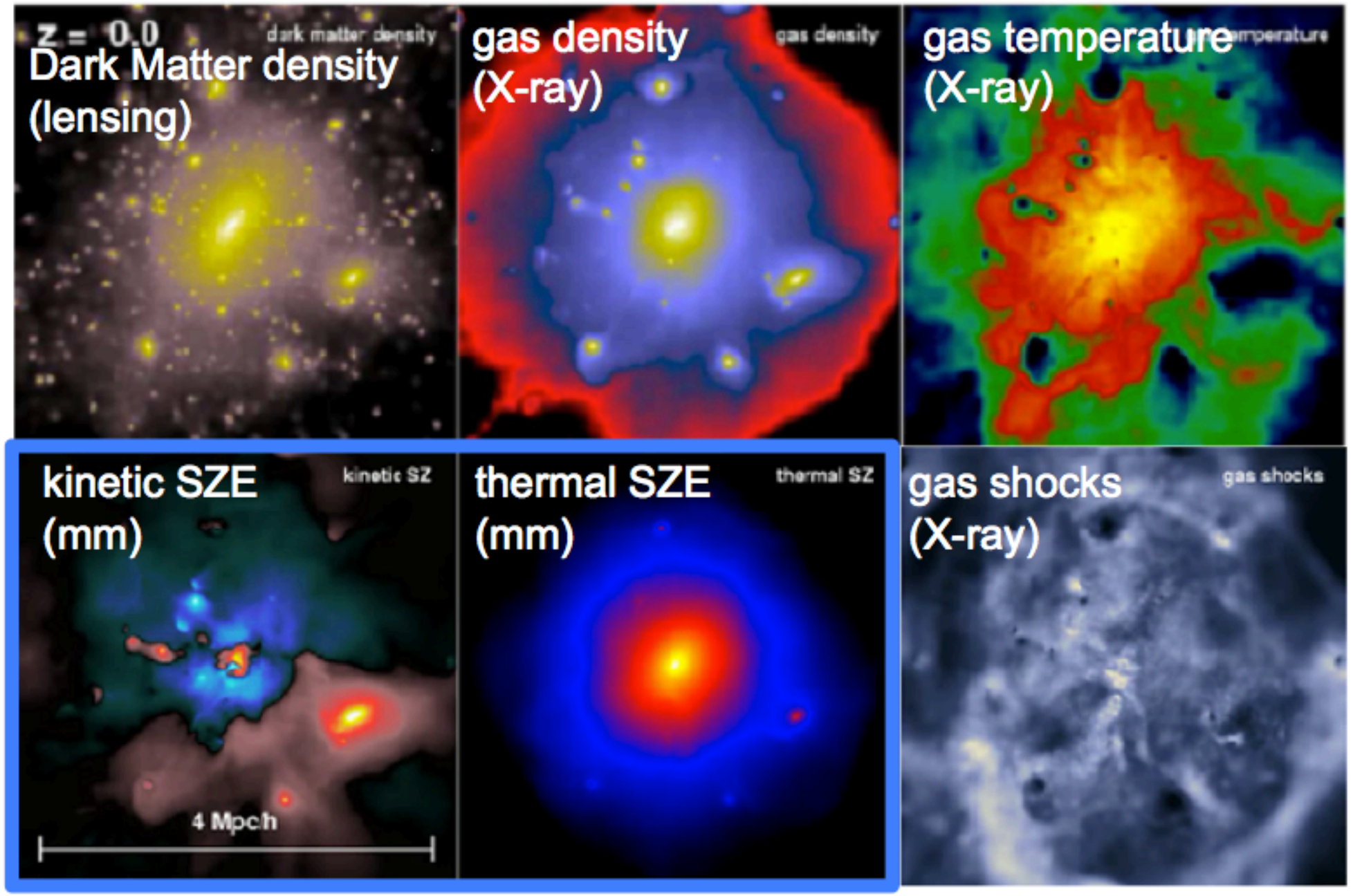

Source: http://www.mpa-garching.mpg.de/galform/data_vis/index.shtml

SZ Experiments

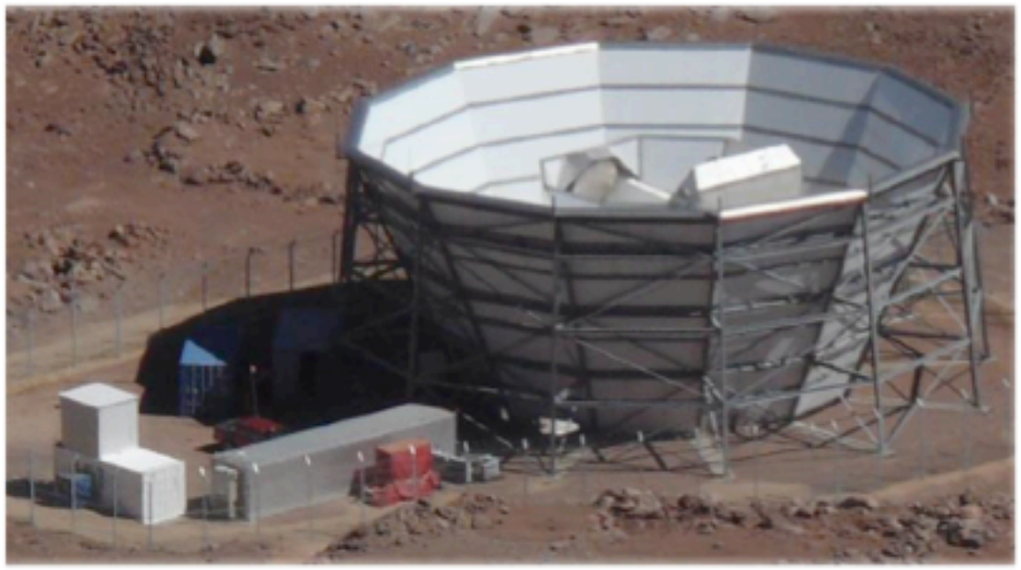

Atacama Cosmology Telescope (ACT)

Location: Cerro Toco (5200m), Chile
Size: 6m
Frequencies: 148, 218, 277 GHz
Resolution: ~1 arcmin
ACT Cluster Survey: ~1000 deg^2

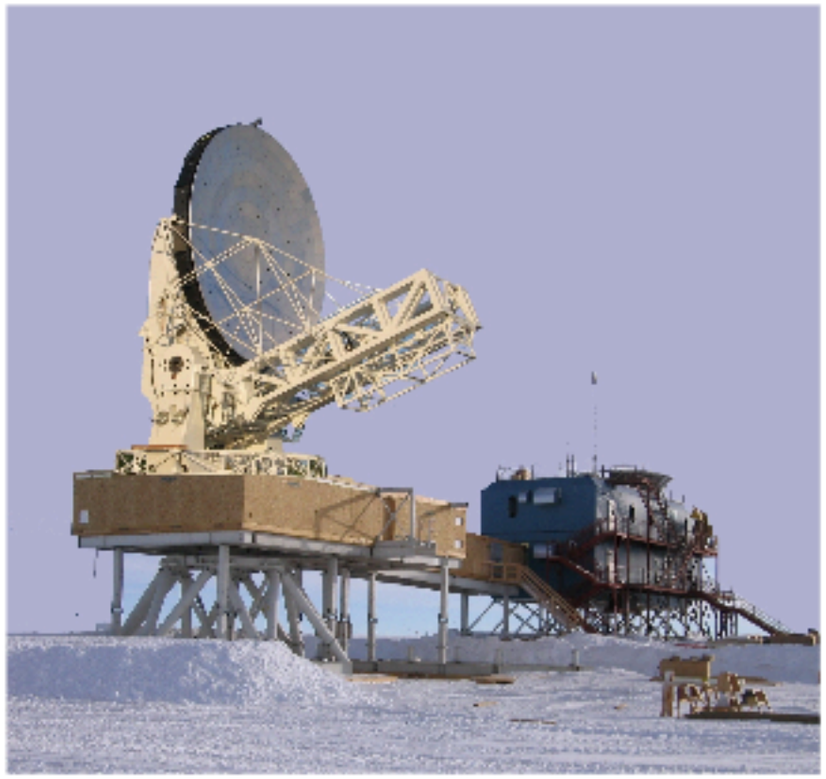

South Pole Telescope (SPT)

Location: SP (2800m), Antarctica
Size: 10m
Frequencies: 90, 150, 220 GHz
Resolution: ~1 arcmin
SPT Cluster Survey: ~2000 deg^2

SZ Experiments

Source: http://planck.cf.ac.uk/results/abell-2319

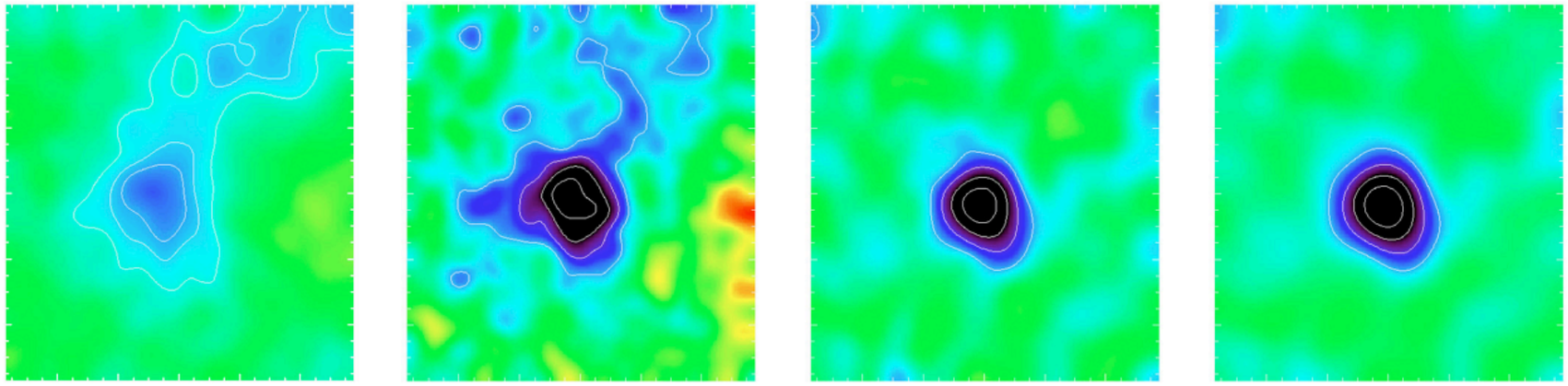

Planck satellite

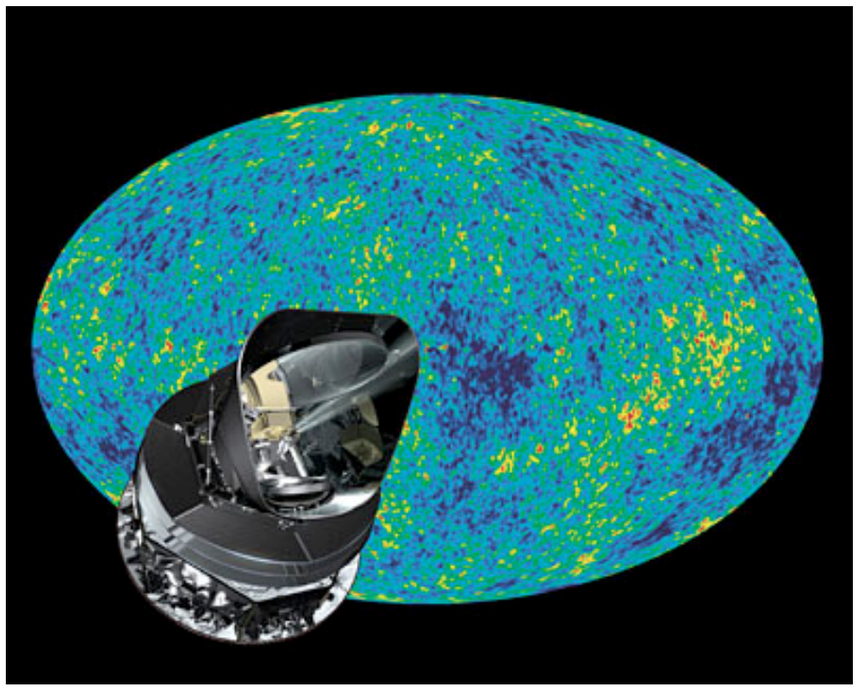

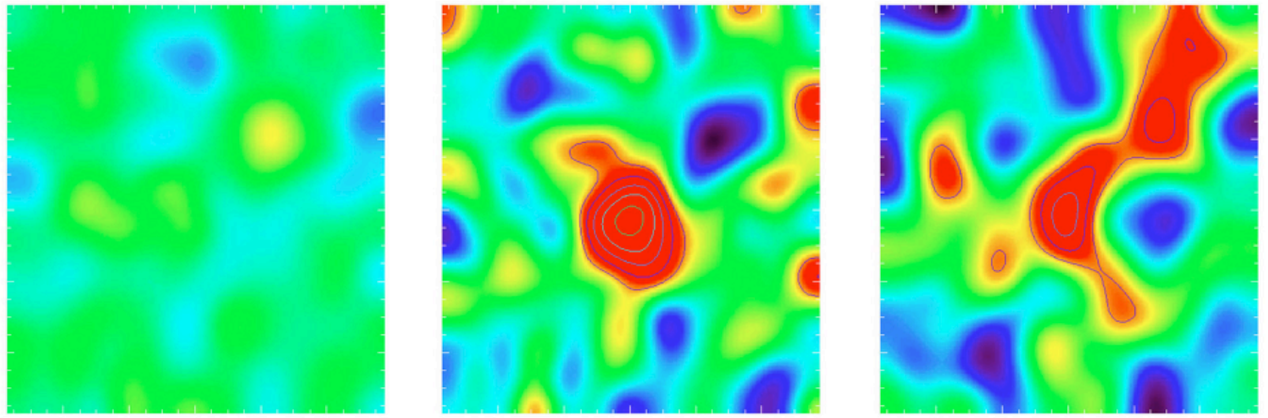

Abell 2319 with PLANCK
Top row: 44, 70, 100, 143 GHz
Bottom row: 217, 353,545 GHz

Some recent SZ results

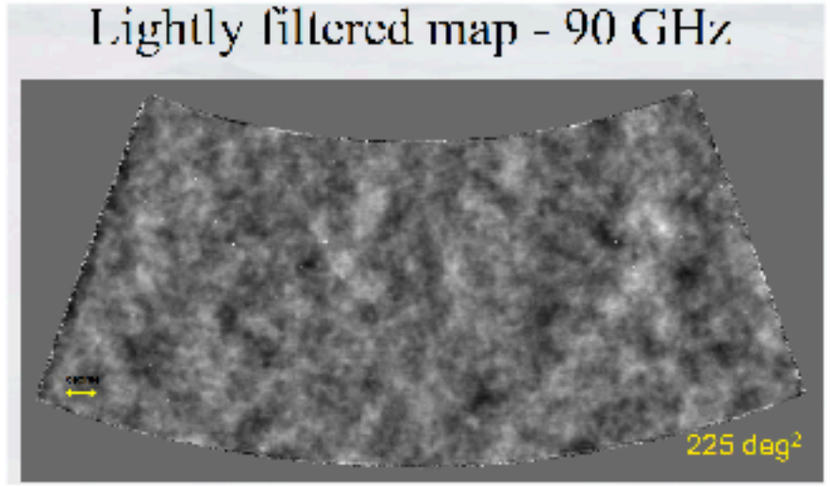

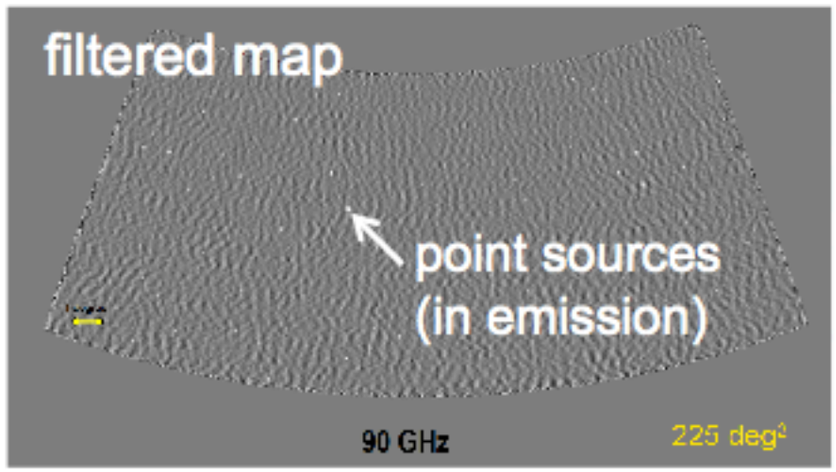

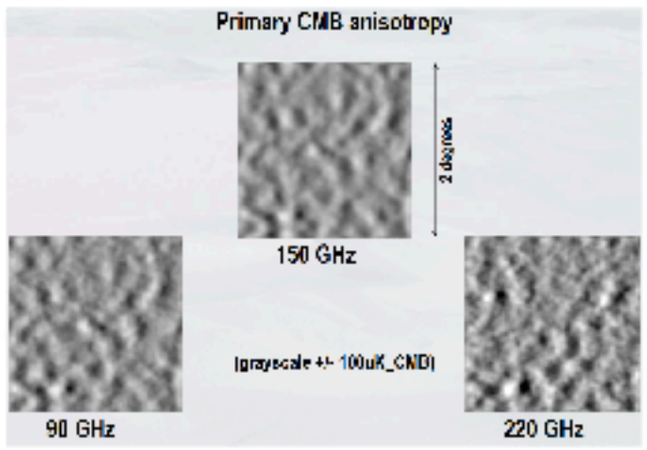

Cluster Finding in Real SPT Observations

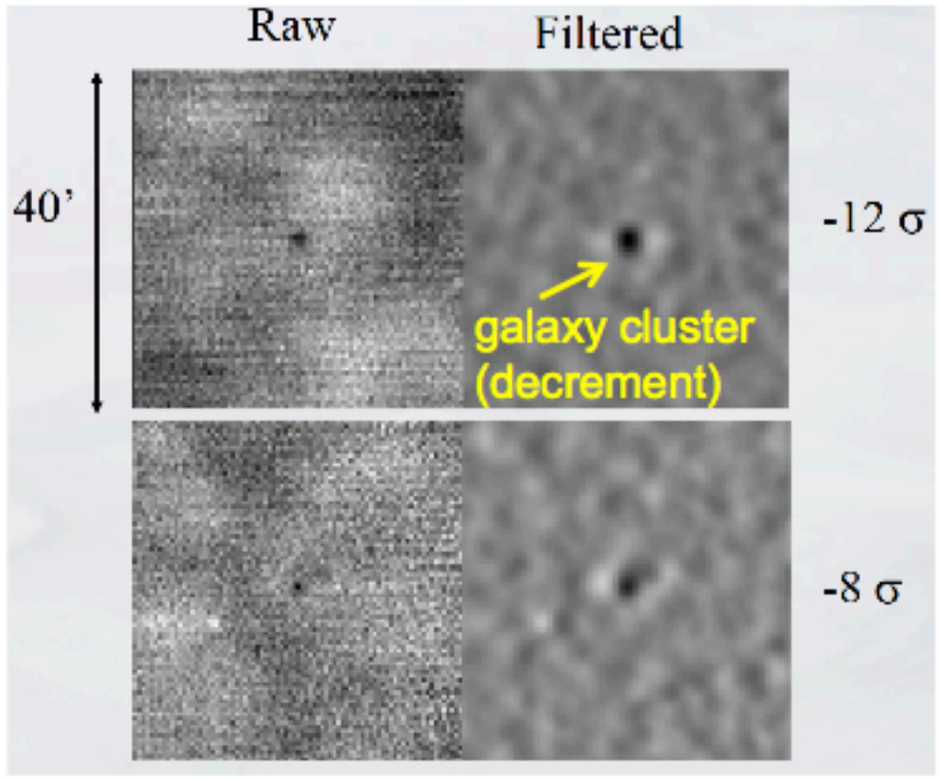

Source: http://member.ipmu.jp/clj2010//program_files/Talks/holzapfel.pdf

Some recent SZ results

The first four SZE discovered galaxy clusters

unfiltered map (with CMB)

filtered detection maps

null maps

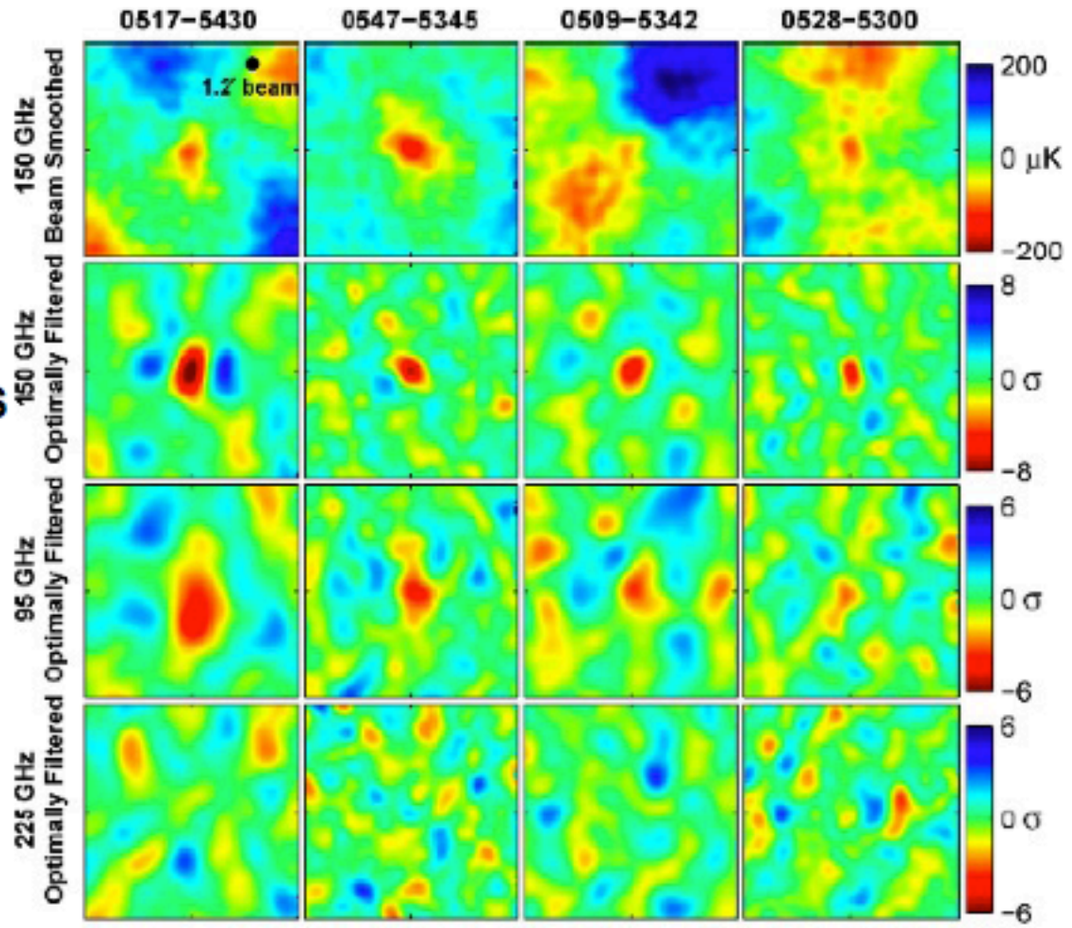

20’x20’ field-of-view

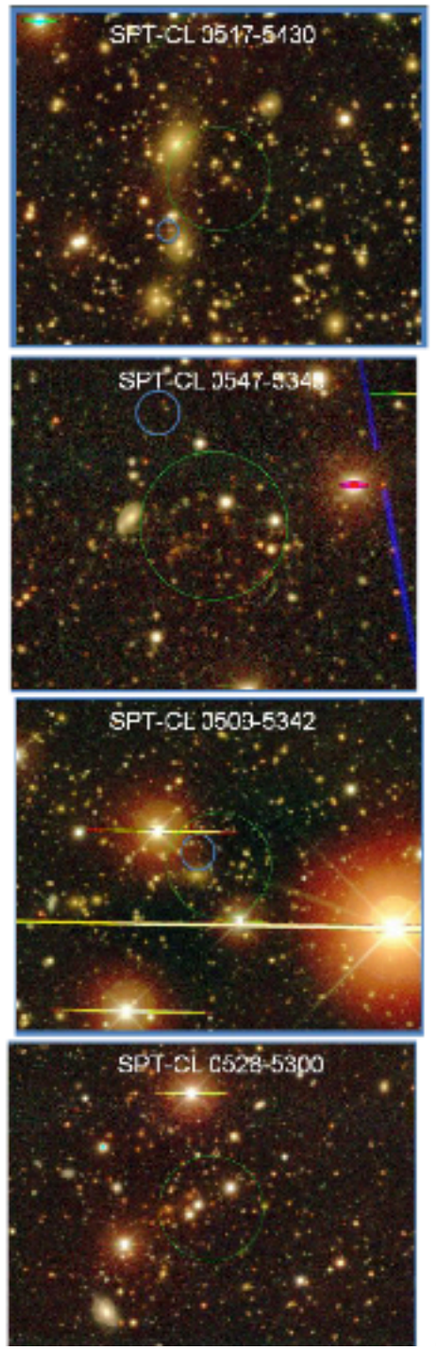

Source: Staniszewski et al. 2009

APEX telescope

- 12-m on-axis ALMA prototype
- Located at the Chilean altiplano, elevation 5100 m
- 1 arcmin reolution @ 150 GHz, 0.4 deg FoV
- Surface accuracy 18 μm

Clusters detected by APEX-SZ

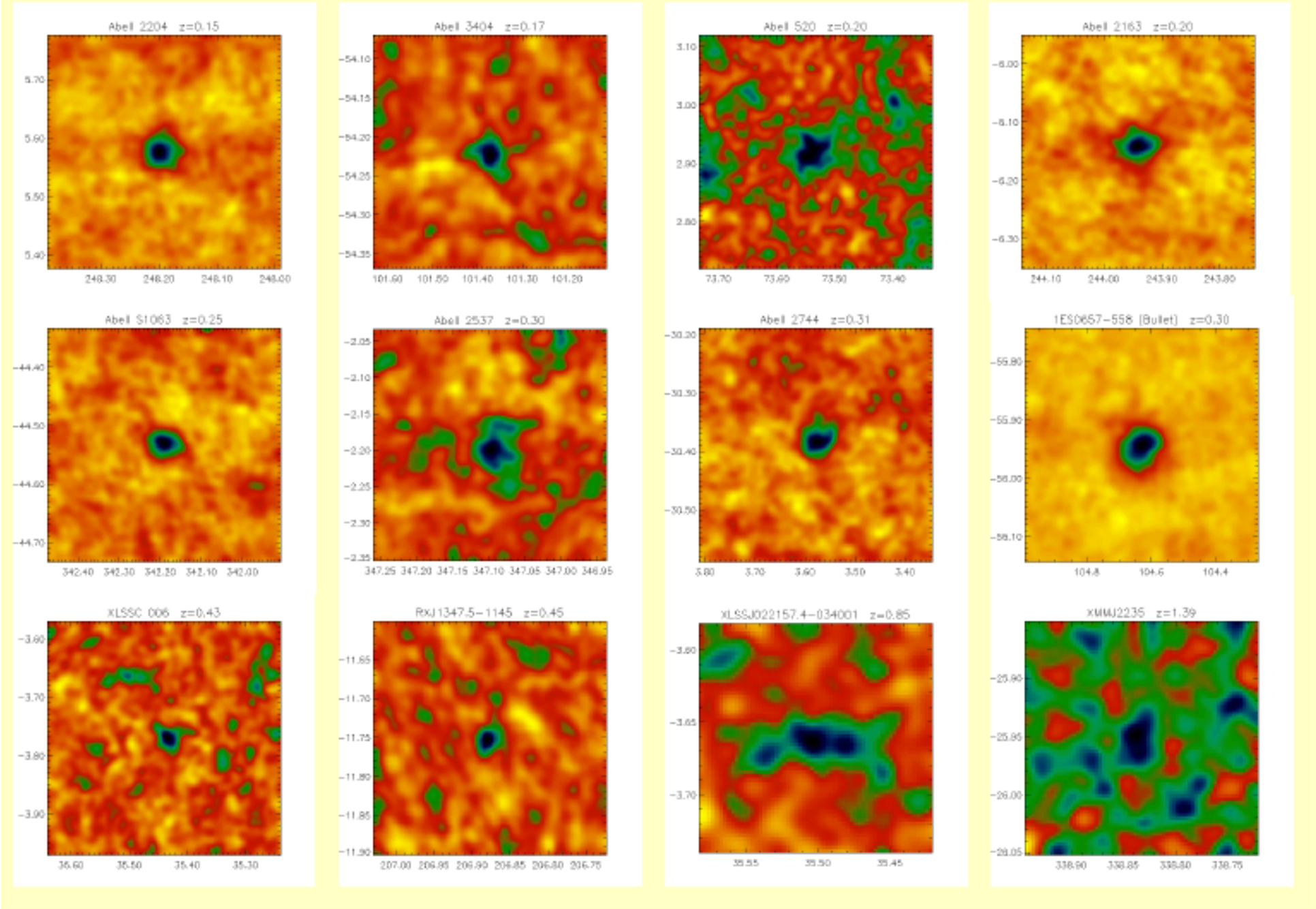

APEX-SZ instrument

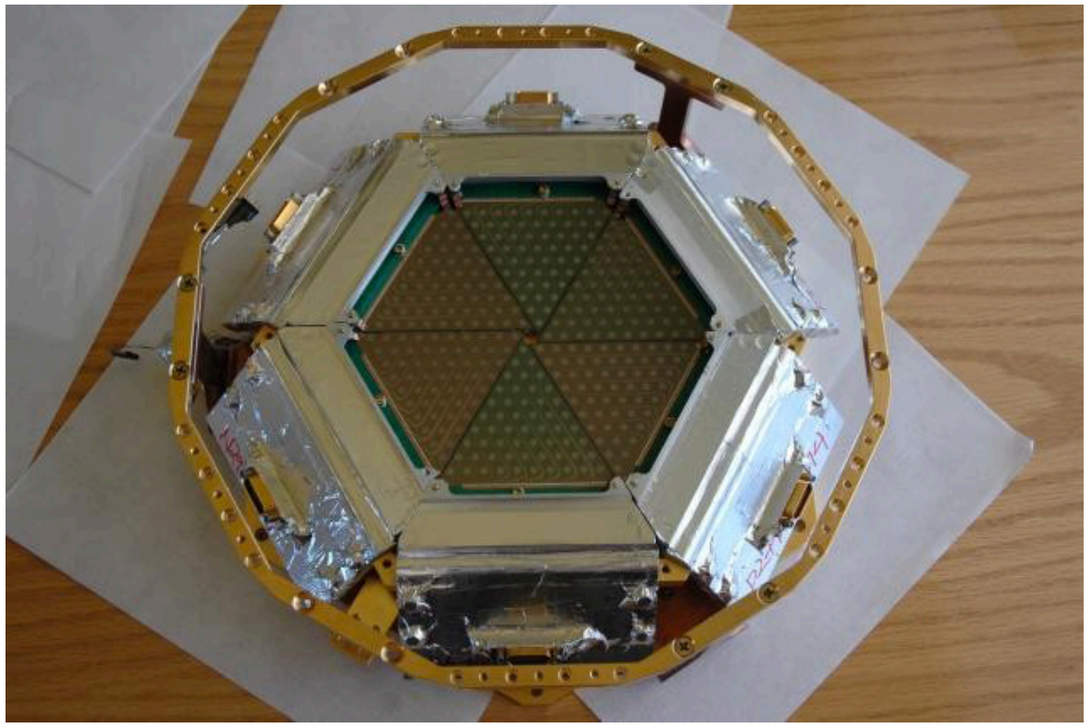

- PI instrument on APEX, commissioned Spring 2007, approx 600 hours of data

- Demonstrates new technologies for SZ experiments:
  - TES bolometers
  - Multiplexed readout electronics
  - Pulse tube cooler (no cryogen loss)

- Can track sources in RA-Dec, powerful camera for targeted cluster observation

ICM and galaxy density profile

- the ICM obeys the baryonic gas physics, so that the ICM density profile $\rho_{gas}(r)$ could be different from that of the DM parent halo
- the easiest physically motivated density distribution is the one for a **self-gravitating sphere of an isothermal gas** with T(r)=T=const
- particles of an isothermal gas have a Maxwellian (MW) velocity distribution
- $\rho_{gas}(r)$ can be derived from:

1. hydrostatic equation + ideal gas equation (as before)

$$-\rho_{\rm gas}(r)\frac{G\,M_{\rm tot}(<r)}{r^2} = \frac{k_{\rm B}}{\mu\, m_{\rm p}}\frac{d[\rho_{\rm gas}(r)\,T_{\rm X}(r)]}{dr}$$

2. plug in T=const, $M(<r) = 4\pi\int r^2\rho(r)dr$, and $k_B T = (\mu m_P)\cdot\sigma_r^2 = const$ which follows from: $\overline{E}_{kin} = \frac{3}{2}k_B T = \frac{1}{2}\langle m\rangle\langle v^2\rangle = \frac{1}{2}\cdot(\mu m_P)\cdot 3\sigma_r^2$
3. rearrange and differentiate both sides to arrive at the differential equation:

$$\sigma_r^2\cdot\frac{d}{dr}\left(\frac{r^2}{\rho(r)}\frac{d\rho(r)}{dr}\right)+4\pi G r^2\rho(r) = 0$$

ICM and galaxy density profile

Singular Isothermal Sphere (SIS) model:

the **Singular Isothermal Sphere (SIS)** is an analytic solution to this differential equation:

$$\rho_{iso}(r) = \frac{\sigma^2}{2\pi G} r^{-2}$$

Properties:

1. singularity for r→0
2. M(r) grows linearly with r → divergent total mass

Reason: MW distribution has a tail with particles at very high velocities; the required gravitationally binding of these particles requires a divergent mass M(r)

ICM and galaxy density profile

King model:

the King Model (King 1966) solves the problem of the divergent total mass

by means of a truncation of the Maxwellian distribution at high velocities, the total mass is only 'logarithmically divergent' (as NFW) and has a flat core:

$$\rho_{King}(r) = \rho_0 \left(1 + \frac{r^2}{r_c^2}\right)^{-\frac{3}{2}}$$

$\mathbf{r_c}$ is the **core radius**, i.e. the characteristic length scale within which the density profile flattens out

$$\rho_{King}(r << r_c) = \rho_0 = const$$

$$\rho_{King}(r >> r_c) \propto r^{-3}$$

ICM and galaxy density profile

The β model:

generalization of the isothermal King models for the approximate description of the X-ray ICM density profile by introducing an additional parameter β :

3d gas profile: $$\rho_{\rm gas}(r) = \frac{\rho_{\rm gas,0}}{\left[1+\left(\frac{r}{r_{\rm c}}\right)^2\right]^{\frac{3\beta}{2}}}$$

$\boldsymbol{\beta}$ is the ratio of the kinetic energies of tracers of the gravitational potential (galaxies) and the mean thermal energies of ICM gas particles:

$$\beta = \mu\, m_{\rm p}\, \sigma_{\rm r}^2/(k_{\rm B} T_{\rm gas})$$

$$\sigma^2_{\rm gal} = \beta\, \sigma^2_{\rm gas}$$

β model of the ICM

A consistently good empirical fit!

$$n_e(r) = n_{e0}\left(1+\frac{r^2}{r_c^2}\right)^{-3\beta/2}$$

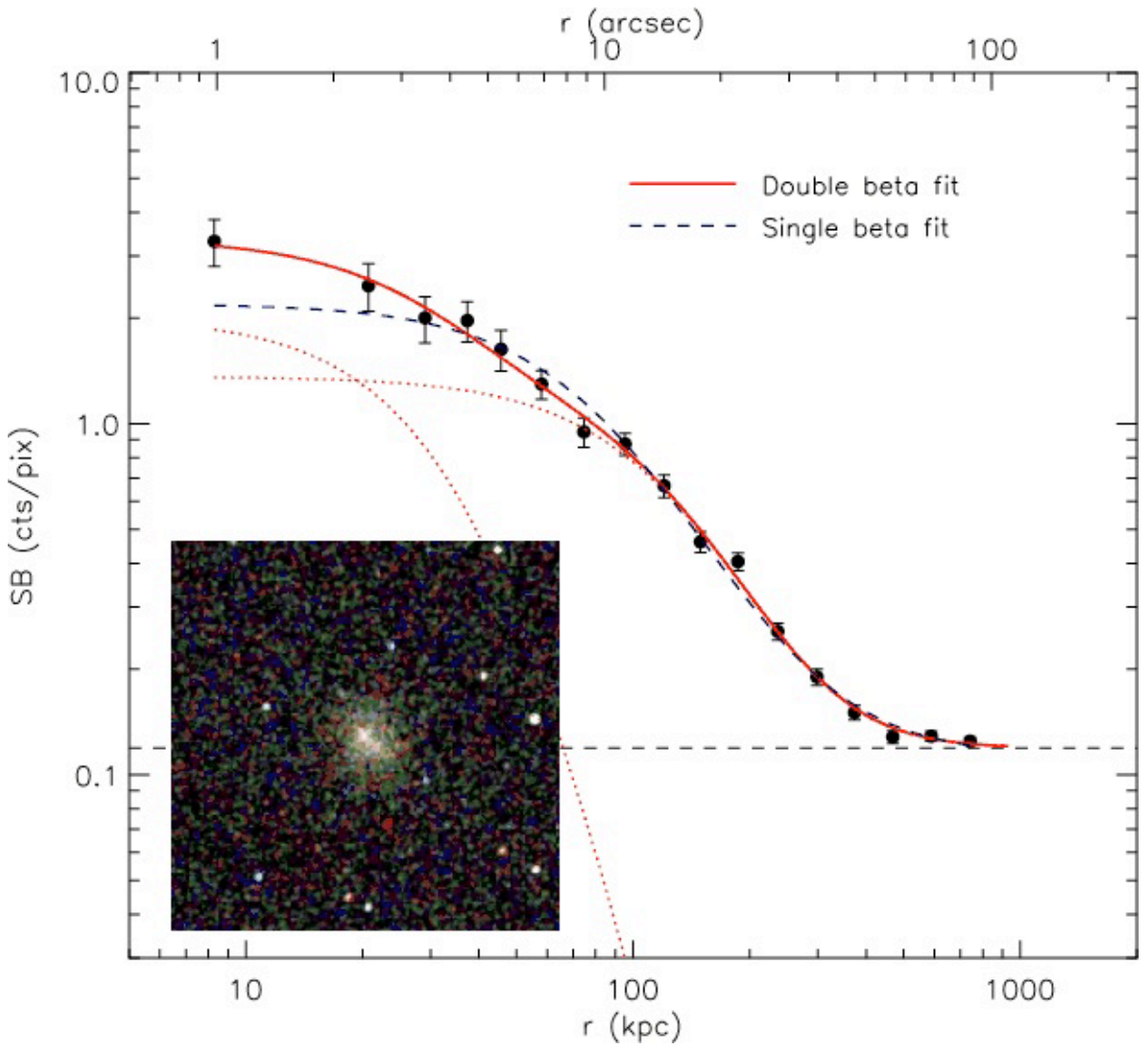

For cool core cluster a much better fit is double β-model

$$n_e(r) = n_{e0}\left[f\left(1+\frac{r^2}{r_{c1}^2}\right)^{-3\beta/2} + (1-f)\left(1+\frac{r^2}{r_{c2}^2}\right)^{-3\beta/2}\right]$$

X-ray and SZ in β-model

The most convenient feature of isothermal β-model is that X-ray surface brightness and SZE decrement takes simple analytical forms

$$S_x = S_{x0}\left(1+\frac{\theta^2}{\theta_c^2}\right)^{(1-6\beta)/2},$$

$$\Delta T = \Delta T_0\left(1+\frac{\theta^2}{\theta_c^2}\right)^{(1-3\beta)/2},$$

Try writing these two expressions in full details by solving these two integrals:

$$\Delta T = f_{(x,T_e)} T_{\rm CMB} D_{\rm A} \int d\zeta\, \sigma_{\rm T} n_e \frac{k_{\rm B} T_e}{m_e c^2}$$

$$S_{\rm X} = \frac{1}{4\pi(1+z)^4} D_{\rm A} \int d\zeta\, n_e n_{\rm H} \Lambda_{e{\rm H}}$$

(integration is along the line of sight $dl = D_A\, d\zeta$)

Solving for n_e

$$n_{e0} = \left\{ \frac{S_{x0} 4\pi (1+z)^4 \mu_H}{\Lambda_{eH} \mu_e} \left[D_A \int \left(1 + \frac{\theta^2}{\theta_c^2} \right)^{-3\beta/2} d\theta \right]^{-1} \right\}^{1/2}$$

$$n_{e0} = \frac{\Delta T_0}{f_{(x,T_e)} T_{\mathrm{CMB}}} \frac{m_e c^2}{\sigma_T k_B T_e} \left[D_A \int \left(1 + \frac{\theta^2}{\theta_c^2} \right)^{-3\beta/2} d\theta \right]^{-1}$$

Integrating over density distribution gives total gas mass:

$$M_{\mathrm{gas}}(r_0) = 4\pi \mu_e n_{e0} m_p \int_0^{r_0} \left(1 + \frac{r^2}{r_c^2} \right)^{-3\beta/2} r^2 dr$$

Solving for d_A

One can solve for the angular diameter distance by eliminating n_{e0} (noting that $n_{\rm H} = n_e \mu_e / \mu_{\rm H}$, where $n_j \equiv \rho / \mu_j m_p$ for species j), yielding

$$D_{\rm A} = \frac{(\Delta T_0)^2}{S_{\rm X0}} \left(\frac{m_e c^2}{k_{\rm B} T_{e0}} \right)^2 \frac{\Lambda_{e{\rm H}0} \mu_e / \mu_{\rm H}}{4\pi^{3/2} f^2_{(x,T_e)} T^2_{\rm CMB} \sigma^2_{\rm T} (1+z)^4} \frac{1}{\theta_c}$$

$$\times \left[\frac{\Gamma(3\beta/2)}{\Gamma(3\beta/2 - 1/2)} \right]^2 \frac{\Gamma(3\beta - 1/2)}{\Gamma(3\beta)} \, ,$$

where $\Gamma(x)$ is the gamma function. Similarly, one can eliminate $D_{\rm A}$ instead and solve for the central density n_{e0}.

More generally, the angular diameter distance is

$$D_{\rm A} = \frac{(\Delta T_0)^2}{S_{\rm X0}} \left(\frac{m_e c^2}{k_{\rm B} T_{e0}} \right)^2 \frac{\Lambda_{e{\rm H}0} \mu_e / \mu_{\rm H}}{4\pi f^2_{(x,T_e)} T^2_{\rm CMB} \sigma^2_{\rm T} (1+z)^4}$$

$$\times \frac{1}{\theta_c} \frac{\int (n_e/n_{e0})^2 (\Lambda_{e\rm H}/\Lambda_{e\rm H0}) d\eta|_{R=0}}{\left[\int (n_e/n_{e0})(T_e/T_{e0}) d\eta|_{R=0} \right]^2} \, ,$$

Reese et al. 2002

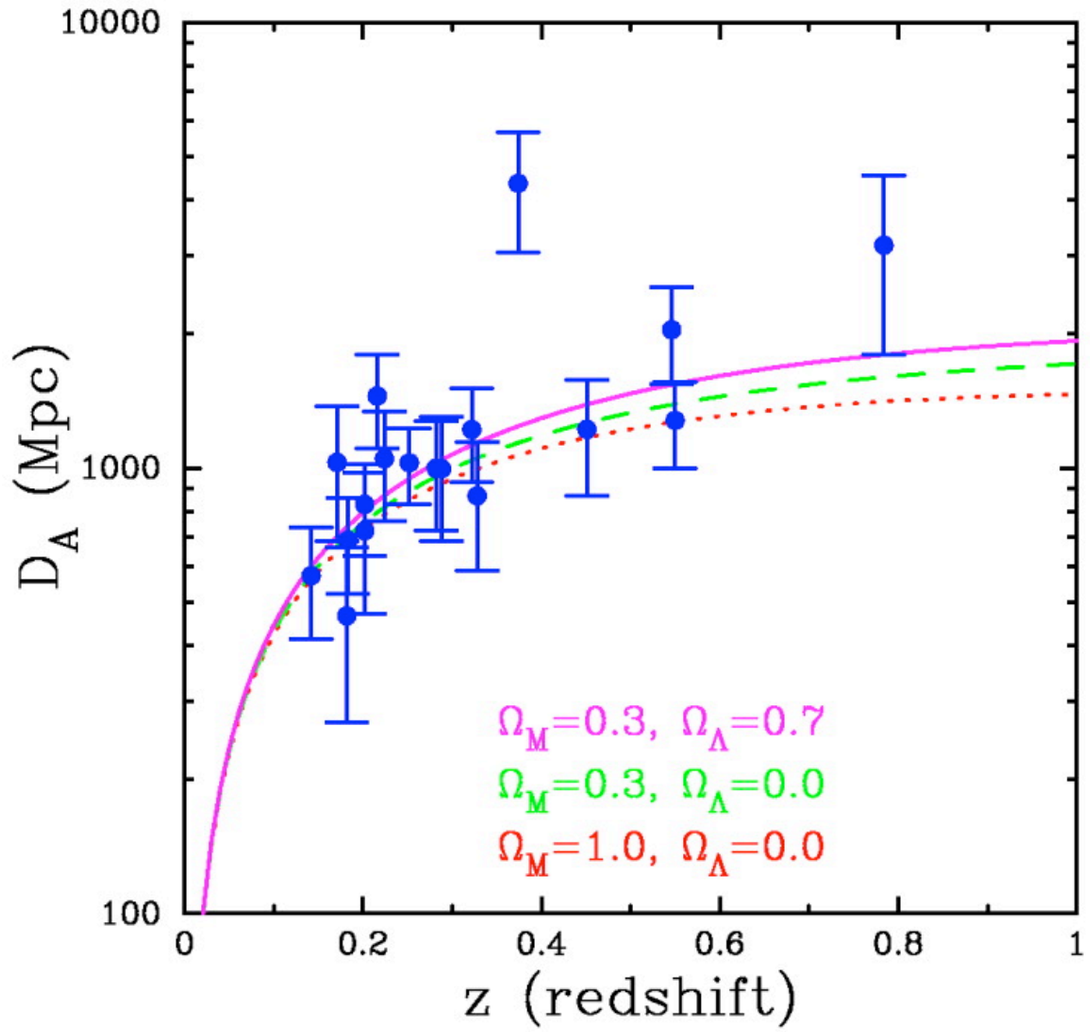

Measuring cluster mass

The condition of hydrostatic equilibrium determines the balance between pressure force and gravitational force: $\nabla P_{\rm gas} = -\rho_{\rm gas} \nabla \phi$.

$$\frac{dP_{\rm gas}}{dr} = -\rho_{\rm gas}\frac{d\phi}{dr} = -\rho_{\rm gas}\frac{GM(<r)}{r^2},$$

Using equation of state for ideal gas:

$$M(<r) = -\frac{r}{G}\frac{k_B T}{\mu m_p}\left(\frac{d\ln\rho_{\rm gas}}{d\ln r} + \frac{d\ln T}{d\ln r}\right),$$

For isothermal beta model:

$$\frac{M(r)}{r} = \frac{3\beta k_{\rm B} T}{G\mu m_p}\frac{(r/r_c)^2}{1+(r/r_c)^2}.$$